

## X-RAY, FUV, AND UV OBSERVATIONS OF $\alpha$ CENTAURI B: DETERMINATION OF LONG-TERM MAGNETIC ACTIVITY CYCLE AND ROTATION PERIOD

L. E. DEWARF<sup>1</sup>, K. M. DATIN, AND E. F. GUINAN<sup>1</sup>

Department of Astronomy and Astrophysics, Villanova University, 800 Lancaster Avenue, Villanova, PA 19085, USA; [Laurence.DeWarf@Villanova.edu](mailto:Laurence.DeWarf@Villanova.edu)  
Received 2009 December 21; accepted 2010 August 11; published 2010 September 20

### ABSTRACT

Over the last couple of decades we have been carrying out a study of stellar magnetic activity, dynamos, atmospheric physics, and spectral irradiances from a sample of solar-type G0-5 V stars with different ages. One of the major goals of this program is to study the evolution of the Sun's X-ray through NUV spectral irradiances with age. Of particular interest is the determination of the young Sun's elevated levels of high-energy fluxes because of the critical roles that X-ray (coronal) through FUV (transition region (TR), chromospheric) emissions play on the photochemical and photoionization evolution (and possible erosion) of early, young planetary atmospheres and ionospheres. Motivated by the current exoplanetary search missions (such as *Kepler* and *CoRoT*, along with the planned *Space Interferometry Mission* and *Darwin/Terrestrial Planet Finder* missions) that are hunting for Earth-size planets in the habitable zones (liquid water) of nearby main-sequence G–M stars, we are expanding our program to cooler, less luminous, but very importantly, much more numerous main-sequence K-type stars, such as  $\alpha$  Centauri B. The long life ( $2\text{--}3\times$  longer than the Sun) and slow evolution of K stars provide nearly constant energy sources for possible hosted planets. This program parallels our “Sun in Time” program, but extends the study to stars with deeper convective zone depths. Presented here are X-ray (coronal; *ROSAT*, *Chandra*, *XMM-Newton*), UV (TR; *International Ultraviolet Explorer (IUE)*), NUV (chromospheric; *IUE*), and recently acquired FUV (TR/chromospheric; *FUSE* Cycles 7/8) observations of the K1 V star  $\alpha$  Cen B (HD 128621;  $V = 1.33$ ;  $(B - V) = +0.88$ ;  $\tau = 5.6 \pm 0.6$  Gyr). These combined high-energy measures provide a more complete look into the nature of  $\alpha$  Cen B's magnetic activity and X-ray–UV radiances. We find that  $\alpha$  Cen B has exhibited significant long-term variability in X-ray through NUV emission fluxes, indicating a solar-like long-term activity cycle of  $P_{\text{cycle}} = 8.84 \pm 0.4$  years. In addition, analysis of the short-term rotational modulation of mean light due to the effects of magnetically active regions has yielded a well-determined rotation period of  $P_{\text{rotation}} = 36.2 \pm 1.4$  days.  $\alpha$  Cen B is the only old main-sequence K star with a reliably determined age and rotation period, and for early K stars, as in the case of the Sun for G2 V stars, is an important calibrator for stellar age/rotation/activity relations.

**Key words:** stars: activity – stars: individual ( $\alpha$  Centauri B) – stars: magnetic field – ultraviolet: stars – X-rays: stars

## 1. INTRODUCTION

### 1.1. The “Sun in Time” Program

Since 1990 we have been carrying out an in-depth study of the evolution of the chromospheres, transition regions (TRs), and coronae of  $\sim 1.0 M_{\odot}$  stars throughout their main-sequence lifetimes (see Dorren & Guinan 1994a, 1994b; Dorren et al. 1994; Güdel et al. 1997, 1998; and more recently, Guinan et al. 2003; Ribas et al. 2005; Guinan et al. 2009). This program, called “The Sun in Time,” is a comprehensive study across the electromagnetic spectrum using a homogeneous sample of single, nearby G0-5 main-sequence stars with known rotation periods and well-determined physical properties (viz., mass, radius, temperature, etc.) These stars are used as proxies for the Sun at different ages, and thereby help to quantify the effects of spin-down due to magnetic braking. This investigation also bears on the crucial question of the influence of the young Sun's strong X-ray and FUV emissions on developing planetary systems—particularly on the photochemical and photoionization evolution of early planetary atmospheres. To this end, we have constructed spectral irradiance tables for the Sun at different ages (see Ribas et al. 2005). These data sets are of great interest to researchers in paleo-planetary atmospheres as well as for

studies of the evolution of the atmospheres for the increasing number (400+ reported as of 2009 December) of planets now found orbiting other stars. For example, we have recently collaborated with an astrobiology group to study the effect of the young Sun's strong X-ray and ultraviolet (XUV) irradiance on the loss of water from Mars and its implications for the oxidation of the Martian soil (Lammer et al. 2003a). In other studies (Lammer et al. 2003b; Grießmeier et al. 2004), our solar proxy data have been used to investigate the atmospheric loss of exoplanets resulting from XUV heating, which can eventually lead to the evaporation of “hot Jupiters.” Kulikov et al. (2006) have used these data to investigate the early evolution and erosion of Venus' atmosphere.

### 1.2. Expanding to the dK Stars

More recently, we have expanded this “Sun in Time” project to include the much more numerous early K-type stars ( $\sim 3\times$  higher space density than G-type stars). The slower evolution of dK stars (due to their lower mass and slower nuclear reaction rates) makes these attractive stars for hosting habitable planets with long-lived, stable climates. The focus of the overall investigation is twofold: (1) Modeling of dwarf K-type stars to better understand magnetic activity and magnetic energy generation (i.e., dynamo), and (2) Constructing complete irradiance tables covering the main-sequence evolution of low-mass K-type stars. Similar to the solar proxies, the

<sup>1</sup> Based on observations made with the NASA–CNES–CSA *Far Ultraviolet Spectroscopic Explorer (FUSE)*. *FUSE* is operated for NASA by the Johns Hopkins University under NASA contract NAS5-32985.

**Table 1**  
Properties of Representative K-type Program Stars

Object Name	HD Number	Sp. Type	$V$ (mag)	$T_{\text{eff}}$ (K)	Dist. (pc)	$P_{\text{rot}}$ (days)	Age (Gyr)	Age Indicator
Sun <sup>a</sup>	...	G2 V	-26.74	5777	1 AU	25.38	4.6	Isotopic Dating
AB Dor <sup>a</sup>	36705	K1 V	6.93	5260	14.9	0.514	0.05	AB Dor Moving Group
V833 Tau	283750	K2 V	8.42	4600	17.9	1.81	0.13	Pleiades Str
HR 08	166	K0 V	6.13	5400	13.7	5.2	0.35	UMa Str
EP Eri	17925	K1 V	6.03	5100	10.4	6.6	0.35	UMa Str
$\epsilon$ Eri <sup>a</sup>	22049	K2 V	3.73	5050	3.22	11.4	0.65	Hyades Str
<i>Hyades Average</i> <sup>b</sup>	...	...	...	...	...	$<11.07 \pm 1.54>$	0.65	Hyades Str
V2215 Oph	156026	K5 V	6.34	4480	5.4	$\sim 18$	$\sim 2.0$	Activity/Rotation Relation
40 Eri A	26965	K1 V	4.43	5300	5.04	$31 \pm 3$	5.1	Age of WD Companion
HR 637 <sup>a</sup>	13445	K1 V	6.12	5240	10.9	30.1	4.5	Age-Activity Relation
$\alpha$ Cen B	<b>128621</b>	<b>K1 V</b>	<b>1.33</b>	<b>5316</b>	<b>1.347</b>	<b><math>36.23 \pm 1.35</math></b>	<b><math>5.6 \pm 0.6</math></b>	<b>Isochrones of <math>\alpha</math> Cen A (Flannery &amp; Ayres 1978)</b>
61 Cyg A	201091	K5 V	5.22	4450	3.4	$\sim 37$	$\sim 6.0 \pm 2$	61 Cyg Moving Group (Eggen 1996)
HR 7703	191408	K3 V	5.31	4893	6.05	$\sim 50$	$10.0 \pm 2$	HV star (Old Disk)

#### Notes.

<sup>a</sup> Star with planet/brown dwarf companion(s): AB Dor  $\approx 93 M_J$ ;  $\epsilon$  Eri  $\approx 0.92 M_J$ ; HD 13445  $\approx 4.2 M_J$ .

<sup>b</sup> Weighted average rotation period value derived from nine K0–K5 V directly measured Hyades members (Radick et al. 1987).

stars in this program have been selected in a narrow spectral type interval (K0–K5 V) and cover a wide range of rotation periods (aka ages). As shown in Table 1, our sample of targets covers ages from  $\sim 50$  Myr ( $P_{\text{rotation}} \approx 0.5$  days) to 8–12 Gyr ( $P_{\text{rotation}} \approx 50$  days). These program stars have well-determined parallaxes, colors, spectral types, and also have observations of age-sensitive measures (rotation) such as  $L_X$ , C IV ( $\lambda 1550 \text{ \AA}$ ), and Mg II  $h+k$  ( $\sim 2800 \text{ \AA}$ ) emission fluxes.

This larger study, besides improving our understanding of magnetic dynamo-related phenomena, will help to identify and characterize stars that might be suitable for life. dK stars are excellent hosts for habitable planets—possessing long life, stability, and slow changes in luminosity with time. Their habitable zones (HZs) are fixed for billions of years. Because of the relatively large number of main-sequence K-type stars ( $\sim 13\%$  of all stellar types) in the solar neighborhood, and the closeness of their habitable regions (0.4–0.8 AU), these stars will likely be the main targets of exoplanet search missions such as *Kepler* and *CoRoT*, along with the proposed *Space Interferometry Mission* and *Darwin/Terrestrial Planet Finder* mission. An additional important attribute of K stars in terms of habitability is that they evolve very slowly and have lifetimes from 2 to 5 times that of the Sun. These investigations will also have a major impact on studies of X-ray through NUV radiation and their effects on the environments of extrasolar planets and possible origin and evolution of extraterrestrial life.

Long-term chromospheric magnetic activity cycle modulations have been optically measured for nearly 100 K stars (see, for example, Baliunas et al. 1995). At this point, however, the coronal X-ray magnetic activity cycles of both G- and K-type stars are largely unknown, with only about three reasonable determinations (see Favata et al. 2008). Presented here is the analysis of the nearest K star,  $\alpha$  Centauri B.

## 2. THE $\alpha$ CENTAURI SYSTEM

The  $\alpha$  Centauri triple star system is the closest star system to the Sun at a distance of  $1.347 \pm 0.003$  pc (The *Hipparcos* Catalog, Perryman et al. 1997; van Leeuwen 2007; Soederhjelm 1999; Pourbaix et al. 1999).  $\alpha$  Cen AB is a well-separated, tidally non-interacting binary system ( $P_{\text{orbit}}^{\text{AB}} = 79.9$  yr; separation  $\approx 23$  AU), consisting of a G2 V (A) and a K1 V (B) star. A third

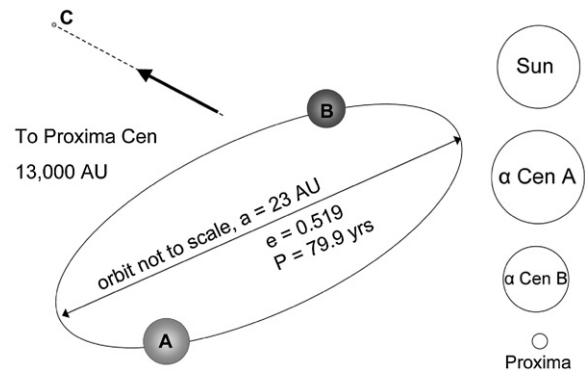


**Figure 1.** Schematic of the  $\alpha$  Cen ABC system is shown above (see also Table 2). The outlines on the right show the Sun and  $\alpha$  Cen's components to scale. The primary component ( $\alpha$  Cen A) is approximately 9% more massive and 22% larger than our Sun, whereas the secondary (B) is about 10% less massive and 14% smaller.  $\alpha$  Cen B is expected to have a deeper and more compact convection zone ( $CZ \approx 0.5 R_*$ ) and is slightly older ( $\tau \approx 5\text{--}6$  Gyr) than our Sun.

component (C), the dM5e star Proxima Centauri, is most likely gravitationally bound to  $\alpha$  Cen AB, but in a wide orbit separated by about 13,000 AU (see Figure 1 and Table 2). The secondary ( $\alpha$  Cen B; HD 128621) is slightly smaller than our Sun with regard to its mass ( $M/M_\odot = 0.90$ ; Demarque et al. 1986; Pourbaix et al. 2002; Yildiz 2008), radius ( $R/R_\odot = 0.86$ ; Kervella et al. 2003), and temperature ( $T/T_\odot = 0.92$ ; Neuforge-Verheecke & Magain 1997; Morel et al. 2000; Porto de Mello et al. 2008). However,  $\alpha$  Cen B is expected to have a deeper convection zone ( $CZ \approx 0.5 R_*$ ) and is slightly older ( $\tau \approx 5\text{--}6$  Gyr; see Flannery & Ayres 1978; Demarque et al. 1986; Guenther & Demarque 2000; Thévenin et al. 2002; Eggenberger et al. 2004; Yildiz 2007, 2008) than our Sun.

Due to its proximity, the  $\alpha$  Cen system has been extensively researched. In studies of stellar magnetic activity,  $\alpha$  Cen forms an astrophysical laboratory to investigate angular momentum loss, coronal and chromospheric activity, for three coeval stars with differing masses (1.09, 0.90, and  $0.12 M_\odot$ ) and deepening outer CZs (0.3, 0.5, and  $\sim 1.0 R_*$ ). Also,  $\alpha$  Cen B is the oldest K-type star with a well-determined age—determined from the isochronal age of its close companion,  $\alpha$  Cen A (5–6 Gyr; Flannery & Ayres 1978). This makes  $\alpha$  Cen B, along with  $\alpha$

**Table 2**  
The  $\alpha$  Centauri System

Property	Sun (Sol)	$\alpha$ Cen A HD 128620	$\alpha$ Cen B HD 128621	$\alpha$ Cen C (Proxima Cen)
Spectral type	G2 V	G2 V	K1 V	dM5e
$V^a$	-26.74	-0.01	1.33	11.05
$(B-V)^a$	0.648	0.71	0.88	1.97
$(b-y)^b$	0.403	0.414	0.524	...
Temperature (K) <sup>c</sup>	5779	5847	5316	~3050
[Fe/H] <sup>d</sup>	$\equiv 0.0$	0.25	0.25	(0.25)
Mass ( $M_\odot$ ) <sup>e</sup>	$\equiv 1.00$	1.09	0.90	0.123
Radius ( $R_\odot$ ) <sup>f</sup>	$\equiv 1.00$	1.22	0.86	0.145
Age (Gyr) <sup>g</sup>	4.58	~5.6	~5.6	~5.6
$P_{\text{rot}}$ (days) <sup>h</sup>	25.38	15–20	36.23 $\pm$ 1.35	~83.1

#### Notes.

<sup>a</sup> Hoffleit & Jaschek (1982).

<sup>b</sup> Crawford et al. (1970; A + B); Eggen (1978b; A, B).

<sup>c</sup> Porto de Mello et al. (2008), cf. Neuforge-Verheecke & Magain (1997), Morel et al. (2000; A, B), and cf. Ségransan et al. (2003; C).

<sup>d</sup> Porto de Mello et al. (2008; A, B); Pettersen (1980; C).

<sup>e</sup> See Eggen (1978a), Halliwell (1981), Demarque et al. (1986), Anosova et al. (1994), Pourbaix et al. (2002), Yildiz (2008; A, B), cf. Ségransan et al. (2003; C).

<sup>f</sup> Kervella et al. (2003; A, B), Ségransan et al. (2003; C).

<sup>g</sup> See Flannery & Ayres (1978), Demarque et al. (1986), Guenther & Demarque (2000), Thévenin et al. (2002), Eggenberger et al. (2004), Yildiz (2007), Yildiz (2008).

<sup>h</sup> Equatorial (Sun), L. E. DeWarf, (2010, in preparation; A), this study (B), Engle et al. (2009; C).

Cen A and  $\alpha$  Cen C (Proxima), crucial calibrators for any age/activity/rotation studies.

The frequency of planets occurring in multiple star systems has recently been investigated by Bonavita & Desidera (2007) and Quintana et al. (2007). In particular, the possibility of planets hosted in the  $\alpha$  Cen AB system has been addressed dynamically by Benest (1988), Wiegert & Holman (1997), and Guedes et al. (2008). In fact, Thebault et al. (2009) show that  $\alpha$  Cen B may be both plausible, and well-suited observationally, for the potential detection of a terrestrial-type planet residing within its habitable zone ( $\text{HZ} \approx 0.6\text{--}1.2$  AU). Unfortunately, to date there is no evidence for planets hosted by the system (see, also, Murdoch et al. 1993; Hatzes et al. 1996; Endl et al. 2001). However, the  $\alpha$  Cen AB system has an  $\sim 2\times$  higher metal abundance than our Sun ( $[\text{Fe}/\text{H}] \approx 0.25$ ; Furenliid & Meylan 1990; Chmielewski et al. 1992; Neuforge-Verheecke & Magain 1997; Doyle et al. 2005; Porto de Mello et al. 2008). This may favor the formation of terrestrial planets. Giménez (2000) and Wyatt et al. (2007), for example, have shown that extrasolar planets tend to be hosted by stars with higher than average metal abundances.

High-precision astrometry of Proxima Centauri ( $\alpha$  Cen C) carried out by Benedict (2008) with the fine guidance sensor (FGS) camera aboard the *Hubble Space Telescope* (*HST*), reveals no evidence of hosted planets with masses greater than  $\sim 5 M_\oplus$  (see also Benedict et al. 1999; Bean et al. 2006; Benedict et al. 2008). However, this study indicated an 83.1 day variation in brightness, most likely originating from the rotational light modulation from starspots. Analysis of over seven years of photometry of Proxima confirms this rotation period (see S. G. Engle et al. 2009, private communication) and also indicates a possible  $\sim 7$  yr starspot cycle. High-precision radial velocity studies have also yielded only upper limits, with  $m \sin i \leq 1 M_\oplus$  and separations  $a \geq 1$  AU (Kürster et al. 1999; Endl & Kürster 2008).

Although the primary focus of this paper is  $\alpha$  Cen B, we now have sufficient data to compare the rotation and activity cycles of all three stars of this system. This comparison is intriguing because all three stars are coeval, differ mainly in mass,  $T_{\text{eff}}$ , and convective zone depth. Thus the  $\alpha$  Cen triple system can serve as a “mini” laboratory for studying angular momentum loss, activity, and cycle properties. As part of our ongoing research, the rotation periods of  $\alpha$  Cen A, B, C are observed to be  $\sim 15\text{--}20$ ,  $36.2 \pm 1.4$ , and  $83.1 \pm 0.6$  days, respectively. As seen, there is a strong dependence of rotation on mass and convective zone depth (magnetic activity). Young ( $\tau < 300$  Myr) G, K, and M stars are for the most part all fast rotators with rotation periods less than about 5 days.

### 3. X-RAY OBSERVATIONS OF $\alpha$ CENTAURI B

The  $\alpha$  Centauri system was observed by the *Röntgen Satellite* (*ROSAT*) High Resolution Imager (HRI; 0.1–2.4 keV), the *Chandra X-ray Observatory* (*Chandra*) Low Energy Transmission Grating Spectrometer (LETGS; 0.07–10 keV with the High Resolution Cameras, HRC-S and HRC-I), and the *XMM-Newton* (*XMM*) European Photon Imaging Camera (EPIC; 0.15–15 keV). Since the range in measured coronal X-ray luminosity depends very strongly on the observed (or chosen) energy band, these luminosity measures cannot be directly compared. Though  $\alpha$  Cen B is a “soft” coronal X-ray source, with no significant amounts of flux expected above about 1 keV, the overall energy passband used/assumed in determining X-ray luminosities is critical.

Fortunately, an important recent study on the  $\alpha$  Cen AB system (along with  $\alpha$  CMi and  $\epsilon$  Eri) by Ayres (2009) nicely resolves this difficulty. In this paper, all spatially resolved measurements from *ROSAT*, *Chandra*, and *XMM* are compared and studied on a common, homogeneous basis, and the appropriate conversion factors for the individual instrumental count rates to absolute fluxes are determined. In our study, all of the original X-ray count rates have been converted into the homogeneous [0.2–2.0 keV] passband using the appropriate energy conversion factors provided by Ayres (2009). Figure 2 displays these combined coronal X-ray luminosities ( $L_X$ ) for both  $\alpha$  Cen A and  $\alpha$  Cen B, respectively. As reported by Ayres (2009), typical uncertainties ( $\Delta L_X$ ) are approximately  $\pm 4\%$ ,  $\pm 3\%$ , and  $\pm 2\%$  for the individual *ROSAT*, *Chandra*, and *XMM* measurements, respectively.

Twenty-seven *ROSAT* pointings were carried out by Jürgen Schmitt in 1996 August/September and show only small-scale variability in the X-ray luminosity levels for  $\alpha$  Cen B, averaging  $L_X = 1.1 (\pm 0.26) \times 10^{27}$  erg s<sup>-1</sup>. At the time of the lone *Chandra* HRC-S observation in 1999 (Raassen et al. 2003), the X-ray luminosity of  $\alpha$  Cen B had slightly increased to  $L_X = 1.9 \times 10^{27}$  erg s<sup>-1</sup>. More recently, the *XMM* observations reported by Robrade et al. (2005) demonstrate that the coronal X-ray luminosity for  $\alpha$  Cen B diminishes from  $L_X = 2.2 \times 10^{27}$  erg s<sup>-1</sup> (early 2004) to  $L_X = 0.3 \times 10^{27}$  erg s<sup>-1</sup> (early 2007)—a factor of  $\sim 7$  in three years’ time. This behavior is directly corroborated by the largely contemporaneously obtained *Chandra* observations (Ayres 2009). As seen in Figure 2,  $\alpha$  Cen B appears near the minimum of a coronal magnetic activity cycle around the early part of 2007.

The range in solar X-ray luminosity also depends strongly on the observed (or chosen) energy band. For example, existing estimations of the long-term variability of the Sun during its  $\sim 11$  year magnetic activity cycle are remarkably varied. The Sun is also a “soft” coronal X-ray source, but the overall energy

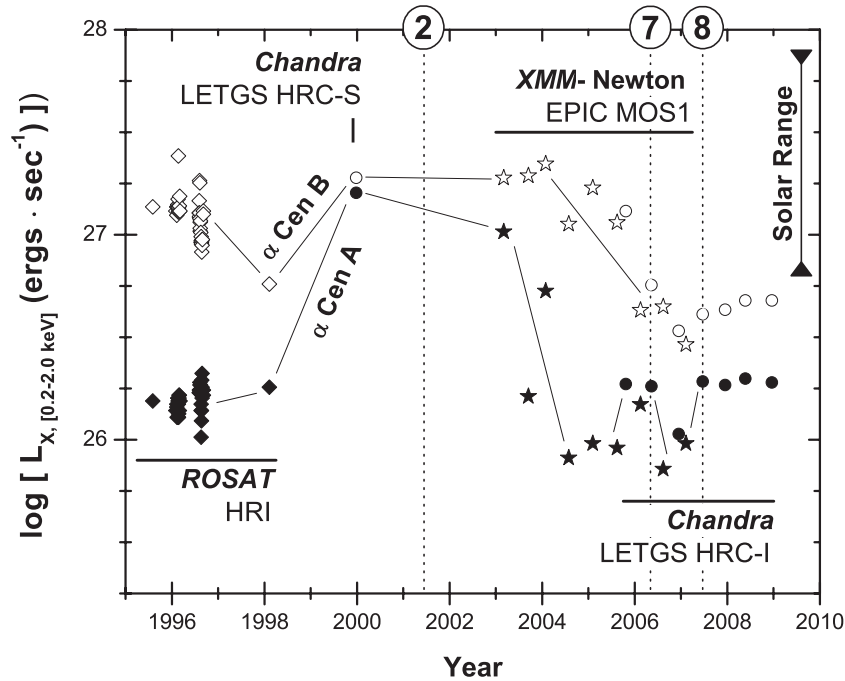


**Figure 2.** Long-term coronal (soft) X-ray light curve of  $\alpha$  Cen A (filled symbols) and  $\alpha$  Cen B (open symbols). The older *ROSAT* (1995–1998; diamonds) and *Chandra* (1999 December; Raassen et al. 2003; circle) observations are combined with the more contemporary *XMM* (2003–2007; Robrade et al. 2005, 2007; stars) and *Chandra* (2005–2008; Ayres 2009; circles) observations. Individual instrumental count rates were converted into the homogeneous (0.2–2.0 keV) passband using the appropriate energy conversion factors provided by Ayres (2009). Typical uncertainties for  $\alpha$  Cen B ( $\Delta \log L_X^B$ ) are  $\pm 0.017$ ,  $\pm 0.010$ , and  $\pm 0.006$ , for the *ROSAT*, *XMM*, and *Chandra* measurements, respectively (Ayres 2009). The vertical dotted lines with indicators along the top show when the *FUSE* Cycles 2, 7, and 8 observations were obtained. Note that the Cycle 7/8 observations coincide closely with a possible low magnetic activity state of  $\alpha$  Cen B. The vertical range bar on the right demonstrates the typical variability seen in the contemporary solar X-ray cycle (Judge et al. 2003), and discussed more completely in the text. Noteworthy is that coronal X-ray maximum of the solar-like G2 V  $\alpha$  Cen A roughly coincides with the minimum level of X-ray activity inferred for the current Sun.

passband used/assumed in determining solar X-ray luminosities remains critical. Using solar measurements from the *Student Nitric Oxide Explorer* (*SNOE*) satellite, Judge et al. (2003) cite an expected true max-to-min variation of order 5–6 $\times$  for the Sun over its full activity range for a typical contemporary cycle. This stems from their analysis, and ultimate removal, of the effects of rotational modulation of active regions on the observed X-ray luminosities. This reduces the total measured X-ray luminosity amplitude (12 $\times$ ; activity cycle + rotational modulation) to that component that represents the changes due to the activity cycle alone (5–6 $\times$ ). In their study, great effort was made to convert the observed bandpass of the *SNOE* solar X-ray photometer (SXP; 0.04–0.6 keV) to that of the *ROSAT* Position Sensitive Proportional Counter (PSPC) bandpass (0.1–2.4 keV; in “*ROSAT* All-Sky Survey” mode).

On the other hand, the *Yohkoh* soft X-ray telescope (SXT; 0.25–4.0 keV) also provides direct solar observations corresponding to those we consider here for  $\alpha$  Cen B. In his study, Acton (1996) determined that the Sun’s activity between 1991 November (near solar maximum) and 1995 September (near solar minimum) exhibited a decline in the full-disk X-rays of greater than a factor of  $\sim 25\times$ , with an accompanying change in average coronal temperature of only 3.3 to 1.5 MK. However, it appears that X-ray energy sensitivity is strongly biased to high-X-ray bandpasses, even though no significant amounts of solar flux are expected above about 1 keV.

An excellent review of previous and current published estimates of the Sun’s X-ray luminosity is contained in the work of Judge et al. (2003). Our Table 3 reproduces much of their effort here. As seen, there is a large range of estimated total variation in the Sun’s coronal X-ray luminosity over its long-term magnetic activity cycle, from about 4–50 $\times$  (max/min).

**Table 3**  
Published Estimates of the Sun’s Long-term Cyclic Variations in X-ray Luminosity (see Judge et al. 2003)

Bandpass (keV)	$\log L_{X,\min}$ (erg s $^{-1}$ )	$\log L_{X,\max}$ (erg s $^{-1}$ )	$L_{\max}/L_{\min}$ Ratio	Ref.
0.15–4.0	26.0	27.4	25.1	1
0.15–4.0	27.0	28.0	10.0	2, 3
0.15–4.0	27.2	27.8	4.0	4, 5
0.04–12.4	25.5	27.0	31.6	6
0.1–4.0	25.6	27.1	32.6	7
0.1–2.4	26.7	27.3	4.0	8
0.2–2.0	26.8	27.4	4.0	9
0.1–2.4	26.0	27.7	50.0	10
0.1–2.4	26.8	27.9	12.6	11

**References.** (1) Pallavicini et al. 1981; (2) Vaiana & Rosner 1978; (3) Golub et al. 1982; (4) Schrijver 1983; (5) Rutten & Schrijver 1987; (6) cf Haisch & Schmitt 1996; (7) Acton 1996; (8) Schmitt 1997; (9) Ayres 1997; (10) Orlando et al. 2001; (11) Judge et al. 2003.

Further, these published ranges do not appear to be correlated to upper/lower energy sensitivities or overall X-ray bandpass. Herein we adopt the result given by Judge et al. (2003). We use their determination of the observed X-ray luminosity of the Sun, converted into the *ROSAT* PSPC bandpass, and extrapolated over the entire activity range of a typical contemporary solar cycle. This overall variability (12 $\times$ ) retains the additional influence of rotational modulation. Since it is not possible to remove all effects of rotational modulation on the observed X-ray luminosities of  $\alpha$  Cen A and B due to incomplete temporal coverage (Figure 2), in this manner a direct comparison with the Sun can still be made.

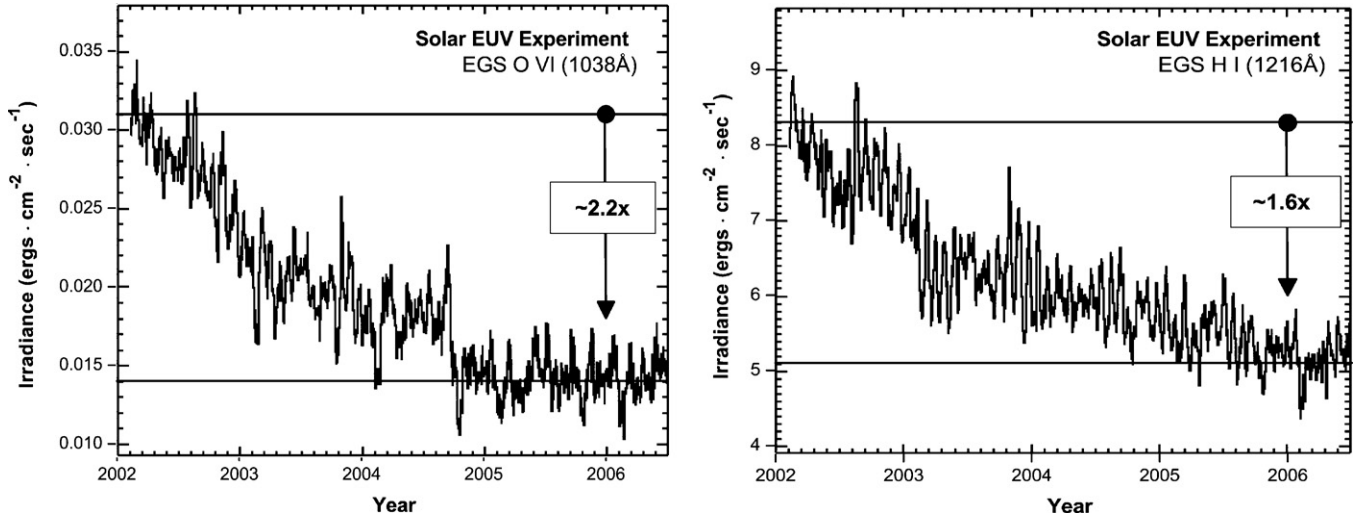


**Figure 3.** Left panel: *SEE* EGS observations of TR-originating O VI emission fluxes for the Sun show a decline of  $\sim 2.2\times$  from near solar max (2002) to solar min. Right panel: the Sun declines by a factor of  $\sim 1.6\times$  in the chromospherically produced H I Ly $\alpha$  emission levels over its  $\sim 11$  year magnetic activity cycle. Both of these declines are primarily due to variations in the overall level of magnetic activity. The Sun is also observed to vary by a factor of about  $\sim 12\times$  in X-ray luminosity (see the text) over the same time frame, thereby exhibiting a high degree of correlation in emission measures throughout its entire atmospheric structure.

Judge et al. (2003) demonstrate that our Sun typically fluctuates in coronal X-ray luminosity by a factor of  $\sim 12\times$  ( $L_X^{\text{Sun}} \approx (6.3\text{--}79) \times 10^{26} \text{ erg s}^{-1}$ ) over its  $\sim 11$  year magnetic activity cycle. Since this X-ray variability is primarily due to changes in the level of overall magnetic activity, not merely coronal temperature changes, the corresponding TR and chromospheric variations are both expected and measured to be tightly correlated (see Lean 1997). Indeed, *Solar EUV Experiment* (*SEE*, on board NASA’s *TIMED* mission; see Woods et al. 2005) observations from 2002 (near solar maximum) to 2006 (solar minimum) show a decline in the TR-produced O VI (1038 Å) emission feature of  $\sim 2.2\times$ , and a decline of  $\sim 1.6\times$  in the chromospheric H I Ly $\alpha$  emission levels (Figure 3).

Studies of cosmogenic isotopes, C<sup>14</sup> (in tree rings) and Be<sup>10</sup> (in ice cores), have been employed to trace the Sun’s activity back over the last  $\sim 12,000$  years (Solanki et al. 2004). Curiously, this study reveals that the solar magnetic activity (defined by solar winds and sunspots) appears to have been exceptionally high over the last  $\sim 70$  years, but is perhaps declining now. This may help to explain the apparently low (relative to the present Sun) coronal soft (0.1–2.5 keV) X-ray luminosities observed for the solar analog  $\alpha$  Cen A, as seen in Figure 2. Three other well-studied solar-type stars (18 Sco, 16 Cyg A and B) also appear to have X-ray emissions considerably lower than current solar values. 18 Sco is the best known match to the Sun with regard to age, rotation, and physical properties, and has an observed  $L_X^{18\text{Sco}} \approx 8 \times 10^{26} \text{ erg s}^{-1}$  at the maximum of its 7–11 year activity cycle (Coughlin et al. 2010). This is comparable to the maximum value of  $L_X$  for  $\alpha$  Cen A, but less than one half of the modern (last two decades) solar values. We have recently been granted *Chandra* X-ray observations of 18 Sco during its activity cycle minimum. Again, as in the case of  $\alpha$  Cen A, this lends support to the hypothesis that the Sun is in an exceptional high activity level compared to historical levels, defined over the last 10,000 years. Although too soon to know for sure, based on previous and current solar activity cycles/measures, the Sun may show signs of declining activity (see Komitov et al. 2010; NOAA Space Weather Prediction Center, [www.swpc.noaa.gov/SolarCycle/](http://www.swpc.noaa.gov/SolarCycle/)).

It is clear that a direct comparison of the Sun to  $\alpha$  Cen B is problematic, since different instruments (and X-ray bandpasses)

are employed for the two disparate objects (see, for example, Micela & Marino 2003). This notwithstanding, the X-ray [0.2–2.0 keV] luminosity of  $\alpha$  Cen B has decreased by a factor of nearly  $7\times$  over the  $\sim 5$  year time frame of the self-consistent *XMM* and/or *Chandra* observations. This behavior thus appears consistent with a solar-like  $\sim 11$  year X-ray activity cycle.

### 3.1. Long-term Coronal X-ray Activity Cycle

The entire  $\alpha$  Cen B X-ray data set spans  $\sim 13$  years (1995–2008) making it potentially sufficient, temporally, to determine the long-term coronal magnetic activity cycle. Therefore, all available X-ray luminosity observations were analyzed using the method of Lomb–Scargle (Lomb 1976; Scargle 1982), as modified for unevenly sampled data (see Horne & Baliunas 1986; Press & Rybicki 1989). This particular algorithm has certain computational advantages over other methods, such as the treatment of missing values and a quantitative estimate of the false discovery rate (FDR). In Section 6 below, additional discussion of the “robustness” of these analytically determined FDRs is given. The results were further refined with an iterative grid search procedure to determine possible cycle rates, modulation amplitudes, and phase information for  $\alpha$  Cen B.

Figure 4 shows the resultant Lomb–Scargle power spectrum for this complete (1995–2008; *ROSAT*, *Chandra*, *XMM*) set of coronal X-ray measurements for  $\alpha$  Cen B. Unfortunately, with only slightly more than one complete cycle’s worth of X-ray data, the long-term magnetic activity cycle length is not well constrained. As seen from the relatively broad nature of the power spectrum, cycle rates of between about 7.5 and 10.75 years must be considered plausible with better than 20% FDR. This notwithstanding, a cycle length of  $P_{\text{cycle}} \approx 8.9$  years is favored with an apparent very high confidence (FDR is essentially 0%).

### 3.2. Short-term Coronal X-ray Modulation–Rotation Period

To determine the rotation period of  $\alpha$  Cen B from the low-amplitude, sinusoidal-like modulation of light due to the rotational effects attributed to the presence of magnetically active regions (starspots, plages, bright light faculae, chromospheric, or coronal features), appropriate sections of data need to be

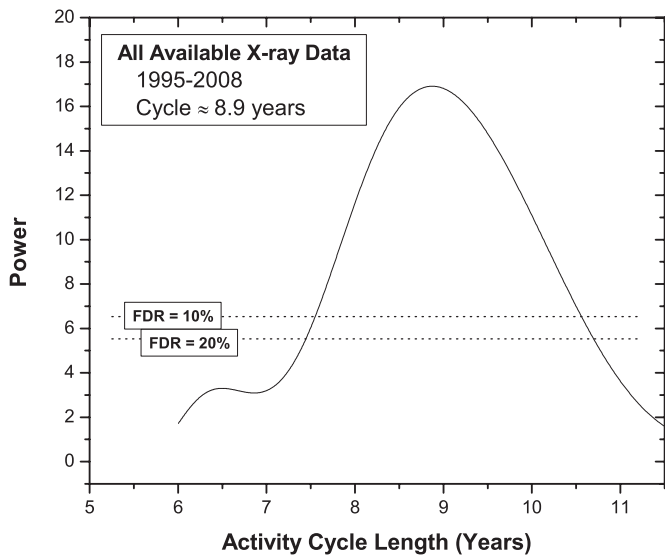


**Figure 4.** Lomb–Scargle power spectrum for all available (1995–2008; *ROSAT*, *Chandra*, *XMM*) X-ray data for  $\alpha$  Cen B. All of the individual instrumental count rates were converted into the homogeneous (0.2–2.0 keV) passband using the appropriate energy conversion factors provided by Ayres (2009). As seen, though cycle rates between 7.5–10.75 years would be plausible with better than 20% FDR, a long-term magnetic activity cycle of  $\sim 8.9$  years is favored with an extremely low FDR. The broad nature of the power spectrum is due to the limited temporal range of data—slightly longer than one complete cycle.

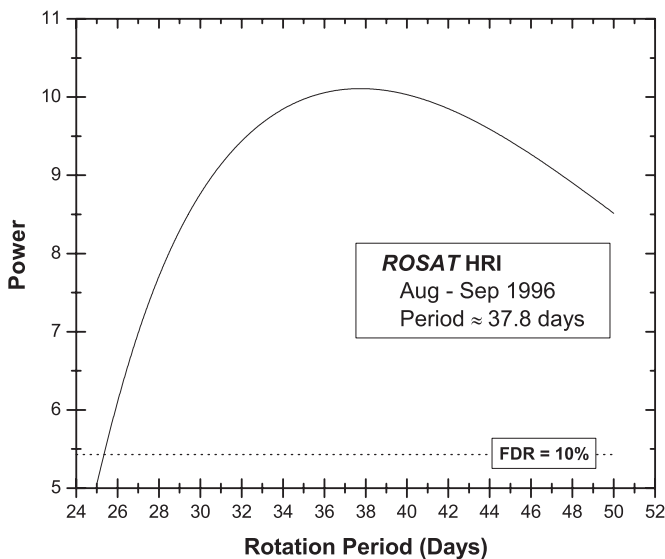


**Figure 5.** Lomb–Scargle power spectrum for the 1996 August–September *ROSAT* HRI X-ray luminosity data for  $\alpha$  Cen B. Apparent in this particular section of data is the modulation of light due to the presence of magnetically active regions. Though there is very high confidence in a  $\sim 37.8$  day rotation period, the broad nature of the power spectrum is due to the limited temporal range of information—less than one complete rotation in length.

isolated. Ideally, suitable portions would be  $\sim 50$ – $100$  days long—long enough to contain sufficient observations, but short enough to minimize the effects of possible formation, migration, and/or destruction of these active regions. Fortunately, the 1996 August–September *ROSAT* pointings contain 27 individual X-ray measures spanning  $\sim 35$  days that should be sufficient for the determination of the rotation period of  $\alpha$  Cen B.

Figure 5 shows the resultant Lomb–Scargle power spectrum for this subsection of *ROSAT* X-ray observations for  $\alpha$  Cen B. As seen, a relatively large range (25.3–50+ days) would result in an estimated FDR better than 10%, but a rotation

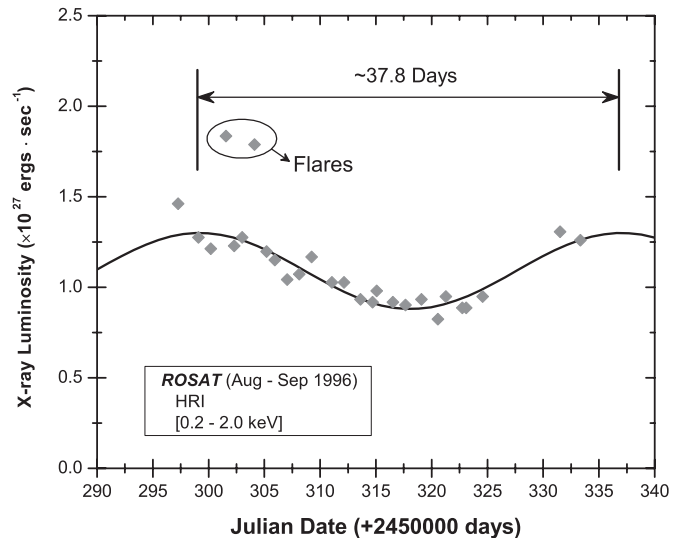


**Figure 6.** 1996 August–September *ROSAT* HRI observations (gray diamonds) shown above are overplotted with the appropriately modulated and phased light curve, as determined utilizing an iterative grid search method and incorporating the  $\sim 37.8$  day rotation period ascertained from the above (see Figure 5) Lomb–Scargle analysis.

**Table 4**  
*FUSE* Observing Log

Object Name	HD Number	Observation Date	Aperture	Exposure (s)
$\alpha$ Cen A	HD 128620	2001 Jun 25	MDRS	15,332
$\alpha$ Cen B	HD 128621	2001 Jun 24	MDRS	22,742
$\alpha$ Cen A	HD 128620	2006 May 5	MDRS	12,606
$\alpha$ Cen B	HD 128621	2006 May 6	MDRS	9245
$\alpha$ Cen A+B	...	2006 May 4	LWRS	5316
$\alpha$ Cen A	HD 128620	2007 Jun 18	MDRS	13,289
$\alpha$ Cen B	HD 128621	2007 Jun 19	MDRS	3565

period of  $P_{\text{rotation}} \doteq 37.8$  days is favored with an apparent very high confidence (FDR  $\approx 0.1\%$ ). Figure 6 shows the 1996 August–September X-ray luminosity observations with the best-fitting, 37.8 day period light curve overplotted. An iterative grid search routine was employed to determine the appropriate light modulation amplitude and cycle phase. In this case, with less than one complete cycle’s worth of information, this rotation period determination cannot be considered well constrained, but in fact is consistent with other independent period estimates (35–42 days) as addressed in more detail below (Section 5.2). As in the case of the Sun, differential rotation of active regions could produce year-to-year variations in observed rotation.

#### 4. *FUSE* FAR-ULTRAVIOLET OBSERVATIONS OF $\alpha$ CENTAURI B

The key emission line fluxes obtained by the *FUSE* satellite are used to probe specific regions of the stellar atmosphere, from the hot plasmas of the upper chromosphere (H I Lyman  $\alpha\beta\gamma\dots$  series;  $\sim 12,000$  K; C II (1036/7 Å),  $\sim 20,000$  K), the TR (C II; C III (977, 1176 Å),  $\sim 50,000$  K; O VI (1032, 1038 Å),  $\sim 300,000$  K) through the low corona (O VI).

The *FUSE* satellite observed both  $\alpha$  Cen A and  $\alpha$  Cen B on three separate occasions (see Table 4). In 2001 June (Cycle 2), both stars were observed with the medium-resolution aperture (MDRS;  $4 \times 20''$ ; Program ID: P104; PI: K. Sembach). The

**Table 5**  
*FUSE* FUV Integrated Emission Fluxes

Atomic Species	Wavelength (Å)	Integration Range (Å)	<i>FUSE</i> Observation Date		
			2001.45	2006.34	2007.47
			Integrated Emission Flux <sup>c</sup>		
C II <sup>a</sup>	1036+7	1036.00–1037.25	1.17 ± 0.68	0.49 ± ...	0.33 ± 0.02
C III	977.020	976.50–977.50	4.12 ± 0.34	1.70 ± 0.37	2.09 ± 0.68
C III <sup>b</sup>	~1176	1174.50–1176.75	2.98 ± 0.60	1.25 ± 0.53	1.11 ± 0.03
O VI	1031.925	1031.50–1032.50	4.15 ± 0.76	1.47 ± 0.49	1.41 ± 0.29
O VI	1037.614	1037.25–1038.00	2.13 ± 0.33	0.63 ± 0.34	0.68 ± 0.22

**Notes.**

<sup>a</sup> Individually combined flux values for the C II doublet at 1036.337 and 1037.018 Å.

<sup>b</sup> Blended fluxes from C III multiplet (six transitions) around 1176 Å.

<sup>c</sup> Integrated emission fluxes units: ( $\times 10^{-11}$  erg cm<sup>-2</sup> s<sup>-1</sup>).

spectra have excellent signal-to-noise ratios (S/Ns) for the stronger emission features, and the peak flux of the C III (977 Å) line for  $\alpha$  Cen B was  $F_{\text{CIII},\lambda 977} = 4.1 \times 10^{-11}$  (cgs). In 2006 May (Cycle 7) and 2007 June (Cycle 8),  $\alpha$  Cen A and B were again observed (ID: G081 and H096; PI: L. DeWarf). At these times, the integrated emission flux values of the same C III emission feature for  $\alpha$  Cen B had diminished to  $1.7 \times 10^{-11}$  and  $2.1 \times 10^{-11}$  (cgs), respectively—dropping by a factor of  $\sim 2.5 \times$  in about five years' time.

The angular separation between  $\alpha$  Cen A and B during the Cycle 7 (2006 May 5) observations had closed to  $9''.53$  along a position angle of  $\theta = 233^\circ$ . Since the failure of two reaction wheels on the *FUSE* spacecraft in 2001 December, this provided some additional difficulties for pointing and acquisition. To obtain separate spectra for  $\alpha$  Cen A and B using the MDRS aperture, the roll angle of the spacecraft needed to be very nearly perpendicular to the position angle of the two stars on the sky—a maneuver rendered significantly more problematic for the crippled satellite. Fortunately, through great effort by the *FUSE* team, the individual spectra of  $\alpha$  Cen A and B were ultimately secured.

All of the  $\alpha$  Cen A and B data were processed in a uniform manner, utilizing the most recent CalFUSE calibration pipeline (version 3.2.0). For consistency, the pre-existing 2001 data have also been reprocessed with this same CalFUSE version. Unfortunately, certain individual exposures obtained no discernable flux from  $\alpha$  Cen B. Another “idiosyncrasy” in the individual exposures were partial flux levels. These anomalously low flux exposures were most likely the result of the star being intermittently contained within the aperture during the duration of the exposure. When examined individually, we found a few of these flawed exposures in the pre-existing 2001 data as well. Therefore, an exposure-by-exposure, segment-by-segment analysis of all of the  $\alpha$  Cen B *FUSE* data was necessitated and all faulty exposures were removed. Fortunately, due to the proximity of the  $\alpha$  Cen system resulting in high received FUV flux values, the S/Ns of the remaining individual “On Target” exposures were excellent.

Table 5 provides the integrated flux values measured for the key FUV emission features for all three of the *FUSE* observing cycles. The uncertainty estimates, stemming from the internal inconsistencies among the individual segments and exposures for a given feature, are also listed. We find that, on average, the individual *FUSE* spectra, secured during a given epoch, are consistent to better than about  $\pm 25\%$ .

Figure 7 shows the comparison between the emission levels for  $\alpha$  Cen B for representative *FUSE* exposures at the three

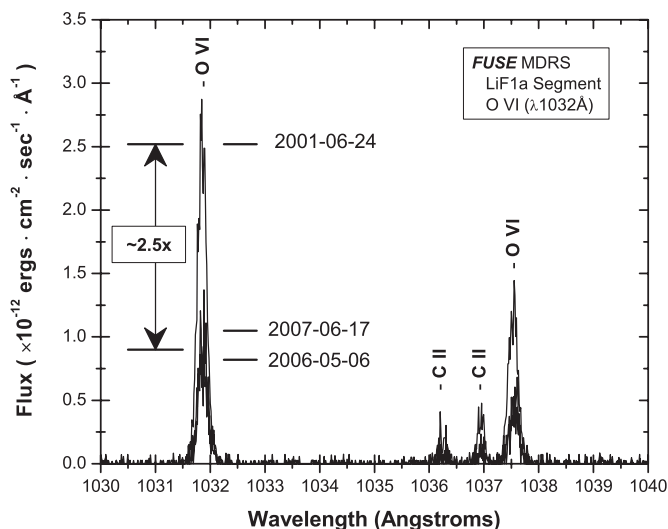


**Figure 7.** Comparison of representative *FUSE* MDRS LiF1a spectra obtained in 2001 June, 2006 May, and 2007 June for  $\alpha$  Cen B. Note the excellent S/N of these individual exposures, though as discussed in the text, the individual *FUSE* spectra, secured during a given epoch, are only internally consistent to about  $\pm 25\%$ . Clearly seen is the significant drop by a factor of  $\sim 2.5 \times$  in the integrated emission fluxes for the TR/chromospheric transitions (O VI, C II) over the five year span from 2001 to 2006. The substantial decline of these key FUV emission measures is likely indicative of a deep-rooted magnetic activity change.

different epochs. Note the substantial decline in integrated FUV flux levels from 2001 June to 2006 May. The ratio of change in these integrated emission flux values, with respect to the 2001 (Cycle 2) values are listed in Table 6. As seen, during the span of time between the Cycle 2 and the Cycle 7/8 observations,  $\alpha$  Cen B diminishes by a factor of  $\sim 2.3$ – $3.3 \times$  in all of these key TR/chromospheric emission measures. Further, the higher temperature transitions (O VI) diminish by a slightly larger amount than the lower temperature transitions (C II, C III). A similar trend is observed during the solar activity cycle (see Lean 1991, 1997; Acton 1996), and it is expected that as  $\alpha$  Cen B becomes less active, changes in starspots, faculae, plages, and magnetic network modify the net radiative output by altering the temperature and density of the otherwise homogeneous stellar atmosphere. Unfortunately, given our estimates for the consistency within the individual *FUSE* spectra, little more can be said about this likely atmospheric temperature trend. The overall drop in FUV emission levels, though, is very likely indicative of a deep-rooted long-term magnetic activity cycle, since variations in atmospheric temperature alone would

**Table 6**  
*FUSE* FUV Integrated Emission Flux Ratios

Atomic Species	Wavelength (Å)	Temperature (K)	Stellar Region	Integrated Emission Flux Ratios	
				(2001.45)/(2006.34)	(2001.45)/(2007.47)
C II <sup>a</sup>	1036+7	~20000	Chromosphere/TR	2.36 ± ...	3.57 ± 2.07
C III	977.020	~50000	TR	2.43 ± 0.56	1.98 ± 0.66
C III <sup>b</sup>	~1176	~50000	TR	2.38 ± 1.12	2.68 ± 0.55
O VI	1031.925	~300000	TR	2.83 ± 1.07	2.92 ± 0.81
O VI	1037.614	~300000	TR	3.37 ± 1.90	3.12 ± 1.12

**Notes.**

<sup>a</sup> Individually combined fluxes from C II doublet at 1036.337 and 1037.018 Å.

<sup>b</sup> Blended fluxes from C III multiplet (six transitions) around 1176 Å.

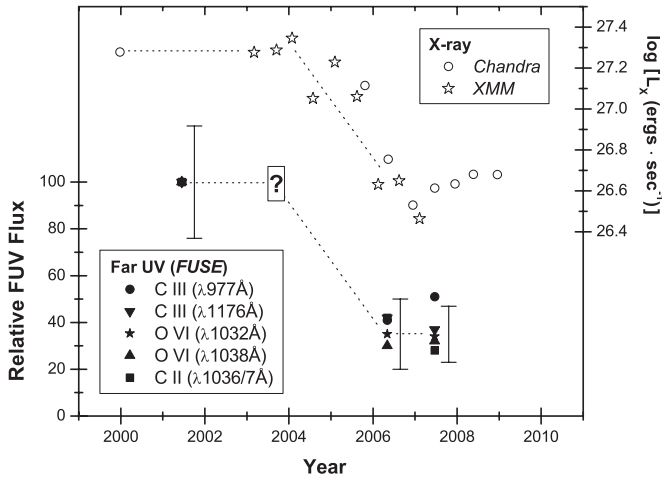


**Figure 8.** Shown in the lower panel above is the relative change in the key FUV emission line fluxes over the three epochs observed by *FUSE* for  $\alpha$  Cen B. All FUV measures are normalized to the 2001 (Cycle 2) observations and the mean individual uncertainty ranges are shown slightly to the right of each epoch. Note the significant drop ( $\sim 2.3$ – $3.3\times$ ) over the five year span from 2001 to 2006 for all of these TR/chromospheric emission features. As expected, there appears to be a slight temperature trend—the higher temperature transitions (O VI) diminish by a potentially larger amount than the lower temperature transitions (C II, C III). That is, as  $\alpha$  Cen B becomes less active its mean atmospheric temperature becomes somewhat cooler. These observed changes in the diagnostic FUV emission line fluxes appear to be in direct accord with the changes taking place in the corona (X-ray; upper panel), pointing to a deep-rooted change in the level of magnetic activity over the possible  $\sim 8.9$  year cycle of  $\alpha$  Cen B.

result in greater departures in the relative differences for the respective atomic species. That is, the reasonably large change in temperature that would be required to alone produce the factor of about  $7\times$  difference in the coronally produced X-ray luminosities presented in Section 3, should also result in a more substantial change in certain FUV temperature sensitive ratios, such as ( $F_{OVI}/F_{CII}$ ). On the other hand, a decline in the overall level of magnetic activity in the star would be expected to reduce commensurately all emission fluxes, as has been addressed above for the case of the Sun.

In Figure 8, the relative fluxes of the key FUV emission lines, as determined with *FUSE*, are displayed over the same time period as the above X-ray observations. This corresponding drop in the FUV emissions, throughout the entire atmospheric structure of the star, indicate a true decrease in the level of magnetic activity, not merely a coronal temperature change.

#### 4.1. Electron Pressures in the Transition Region

We carried out measurements of TR plasma electron pressures ( $P_e$ ) using the same method described by Guinan et al. (2003)

in a *FUSE* study of solar analogs. One interesting preliminary result for  $\alpha$  Cen B, derived from our analysis of the TR electron density sensitive  $\mathcal{R} \equiv F_{CIII,\lambda 1176}/F_{CIII,\lambda 977}$  emission line ratio, infers that the  $P_e$  appears to remain essentially unchanged during the decline in magnetic activity defined by the X-ray fluxes from 2001 to 2006, but then drops significantly from 2006 to 2007, during magnetic quiescence. We find that at the magnetic activity “high-state” of 2001,  $\mathcal{R} \approx 0.28$ , resulting in a  $\log P_e \approx 14.15$  (cgs). At the beginning of the “low-state” in 2006,  $\mathcal{R} \approx 0.29$ , but then appears to abruptly decrease to  $\mathcal{R} \approx 0.16$  by 2007, resulting in an inferred lower electron pressure,  $\log P_e \approx 13.5$  (cgs).

By comparison, the “active” Sun (by measuring discrete active regions of the Sun, such as sunspots/plage regions) has an estimated C III  $\mathcal{R}$ -value of about 0.44 (Noyes et al. 1985; Doyle et al. 1985), with the “quiet” Sun at 0.29 (Dupree et al. 1976). Curiously, the proportional change for both  $\alpha$  Cen B and the Sun are comparable, i.e., ( $\mathcal{R}_{active}/\mathcal{R}_{quiescent}$ )  $\approx 1.67$ . It should be kept in mind, though, that these *FUSE* measures of  $\mathcal{R}$  are integrated over the star’s visible disk and would therefore be influenced by the distribution and the number of active emitting regions of differing sizes and activity strengths.

It would have been interesting to confirm this result for  $\alpha$  Cen B and follow possible  $P_e$  changes over more of this star’s activity cycle, but with the demise of the *FUSE* satellite, this will no longer be possible in the FUV bandpass.

#### 5. ULTRAVIOLET OBSERVATIONS OF $\alpha$ CENTAURI B

The *International Ultraviolet Explorer* (*IUE*) satellite covered wavelengths from 1150 to 3200 Å, allowing us to analyze changes in the prominent C IV (1550 Å) and Mg II  $h+k$  ( $\sim 2800$  Å) emission features from  $\alpha$  Cen B. The C IV emission occurs at temperatures from 50,000 to 100,000 K, typically found in the TR of the star. Mg II (8000–12,000 K) typically originates in the stellar chromosphere. The longevity of the satellite results in a very large data set of UV spectral data, critical to long temporal studies. We have utilized observations from 1978 August to 1995 July, providing us with an extensive timeline of C IV and Mg II information.

For  $\alpha$  Cen B, there are  $\sim 90$  low-dispersion ( $\sim 6$ – $7$  Å), large aperture ( $9 \times 22''$ ) *IUE* spectra obtained by the satellite’s short wave primary (SWP; 1150–1980 Å) camera. Focusing on changes in the TR-produced C IV (1550 Å) emission line over time, the spectra were reduced by first quadratically interpolating the intensity to each integer wavelength. Next, the center of the C IV line core was ascertained by searching for the maximum intensity value between the wavelength range of 1530 and 1565 Å. The flux was then summed over

**Table 7**  
IUE C IV Integrated Emission Line Flux Values

SWP LL <sup>a</sup> Seq. No.	Julian Date (+2440000 days)	Integrated CIV Flux ( $\times 10^{-12}$ cgs)	SWP LL <sup>a</sup> Seq. No.	Julian Date (+2440000 days)	Integrated CIV Flux ( $\times 10^{-12}$ cgs)	SWP LL <sup>a</sup> Seq. No.	Julian Date (+2440000 days)	Integrated CIV Flux ( $\times 10^{-12}$ cgs)
SWP02320	3737.959	1.53	SWP19772	5445.297	1.51	SWP38115	7925.409	1.15
SWP09035	4377.873	1.64	SWP19837	5452.462	1.82	SWP39442	8115.062	1.40
SWP09818	4468.679	0.44	SWP19839	5452.522	1.13	SWP40690	8283.598	0.84
SWP09928	4479.767	1.21	SWP19882	5457.317	0.68	SWP42233	8481.140	1.23
SWP10016	4488.001	0.83	SWP19885	5457.411	1.54	SWP54631	9845.357	2.23
SWP10093	4495.008	1.19	SWP19886	5457.437	1.32	SWP54647	9847.250	2.99
SWP10164	4500.007	0.14	SWP19912	5461.205	1.55	SWP54673	9851.222	2.41
SWP10193	4503.913	1.26	SWP19915	5461.315	1.53	SWP54724	9859.348	0.95
SWP10214	4507.016	0.95	SWP19950	5465.213	1.49	SWP54744	9862.267	1.31
SWP13887	4729.243	1.10	SWP19953	5465.326	1.34	SWP54793	9867.384	1.75
SWP13988	4742.330	1.27	SWP20015	5472.325	0.88	SWP54844	9871.317	1.65
SWP14038	4748.399	0.89	SWP20018	5472.429	1.81	SWP54975	9879.303	2.11
SWP14202	4762.165	2.47	SWP20019	5472.456	1.37	SWP55042	9887.234	1.96
SWP14256	4770.169	0.49	SWP20064	5479.397	1.34	SWP55051	9889.205	1.54
SWP14302	4778.165	1.29	SWP20066	5479.468	0.97	SWP55060	9891.155	2.26
SWP16922	5097.375	2.35	SWP20088	5483.311	1.06	SWP55114	9894.225	0.35
SWP16997	5109.428	1.07	SWP20140	5489.344	1.42	SWP55178	9900.169	1.79
SWP17027	5113.416	1.12	SWP20141	5489.371	1.34	SWP55233	9908.106	0.33
SWP17697	5197.129	1.54	SWP28488	6596.263	2.51	SWP55234	9908.166	2.33
SWP19478	5411.515	3.03	SWP28489	6596.291	1.80	SWP55269	9912.140	2.37
SWP19663	5431.350	0.86	SWP30092	6809.515	2.12	SWP55307	9915.995	1.98
SWP19664	5431.378	1.23	SWP30100	6810.569	3.13	SWP55338	9920.172	1.97
SWP19702	5435.459	0.48	SWP35607	7579.908	1.99	SWP55357	9924.103	1.55
SWP19705	5435.543	1.44	SWP35608	7579.934	1.29	SWP55377	9928.172	1.79
SWP19727	5439.473	1.26	SWP36037	7636.431	1.52	SWP55405	9932.069	1.52
SWP19729	5439.536	1.14	SWP36808	7746.006	0.05			

**Note.** <sup>a</sup> IUE short wavelength primary camera, low dispersion, large aperture.

a 16 Å swatch around this peak value ( $\pm 8$  Å), resulting in integrated flux values for the C IV line, combined with the contribution of the continuum in this bandpass. To account for, and ultimately remove, this continuum flux from the C IV data, an average of the total flux of two bracketing 16 Å swatches (1500–1516 Å and 1582–1598 Å) was then subtracted from the above line+continuum flux. This provided us with an accurate determination of the integrated C IV line emission for  $\alpha$  Cen B. Figure 9 diagrams both the C IV feature and the swatches used to determine the integrated line and continuum fluxes with a typical IUE SWP low-dispersion, large-aperture spectra. Table 7 lists the complete results.

To analyze temporal variations in the chromospherically produced Mg II  $h+k$  (2803+2796 Å) emission features over the same timeline, this study also included ~60 high resolution (0.1–0.3 Å), large aperture (10 × 23") spectra from the IUE satellite's long wave primary (LWP) and long wave redundant (LWR) cameras. Due to differences in the profile of these spectral features, it was necessary to reduce these data in a different manner. We used fixed wavelength regions to define the individual Mg II  $h+k$  line cores and three separate swatch regions. An Mg II "Index" was defined by dividing the integrated flux values for each line by a combination of the three continuum swatches, i.e.

$$\text{Mg II } h+k \text{ emission index} = \frac{h+k}{S}, \text{ where } S = \left( \frac{S_1 + 2S_2 + S_3}{4} \right).$$

In the above relation, the values  $h$  and  $k$  refer to the total integrated flux in the region of the emission features, 2802.4–2804.0 Å and 2795.3–2796.9 Å, respectively. The three swatches are defined to be  $S_1$  (2792.6–2794.2 Å),  $S_2$  (2798.0–2799.6 Å), and  $S_3$  (2805.0–2806.6 Å). The swatch  $S_2$

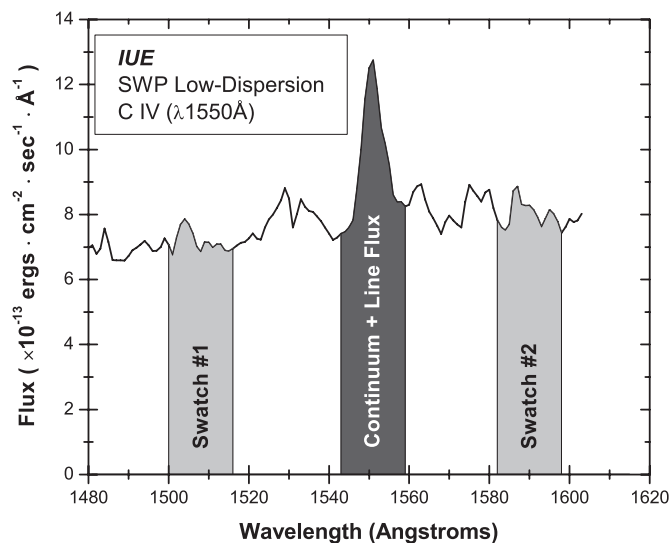


**Figure 9.** Shown above is a typical IUE SWP low-dispersion spectra of  $\alpha$  Cen B that diagrams the swatches (as discussed more completely in the text) used to determine the integrated line and continuum fluxes for the C IV (1550 Å; 50,000–100,000 K; TR) emission feature.

is not centered directly between the  $h+k$  features to avoid the fiducial mark (reseau) incorporated into the IUE vidicon detector. An example of this method for measuring the Mg II  $h+k$  emission line strength is shown in Figure 10 and Table 8 lists the complete results.

The IUE vidicon cameras had a maximum dynamic range of 256, though this was significantly limited by background noise and a low-level baseline intensity "pedestal." Ayres (1993) point

**Table 8**  
*IUE* Mg II *h+k* Emission Indexes

LWP/R HL <sup>a</sup> Seq. No.	Julian Date (+2440000 days)	Mg II <i>h+k</i> Index	LWP/R HL <sup>a</sup> Seq. No.	Julian Date (+2440000 days)	Mg II <i>h+k</i> Index	LWP/R HL <sup>a</sup> Seq. No.	Julian Date (+2440000 days)	Mg II <i>h+k</i> Index
LWR02095	3737.873		LWR12908	5059.353		LWP30740	9859.341	7.63
LWR02096	3737.898	8.96	LWR12909	5059.384		LWP30763	9862.311	7.99
LWR02097	3737.919		LWR13193	5097.379	7.71	LWP30835	9871.311	9.96
LWR08526	4468.691		LWR13220	5100.398	9.50	LWP30863	9879.299	10.40
LWR08640	4479.760	11.01	LWR13221	5100.428		LWP30916	9887.261	8.28
LWR08722	4487.996	9.32	LWR13222	5100.463		LWP30930	9889.233	8.00
LWR08778	4495.006	9.49	LWR13277	5109.425	7.28	LWP30940	9891.134	7.26
LWR08830	4500.004	7.83	LWR13303	5113.413	6.12	LWP30946	9894.202	9.82
LWR08858	4503.910	8.23	LWR13958	5197.127		LWP30962	9900.163	8.75
LWR08884	4507.013	8.83	LWR15736	5439.566	7.17	LWP31015	9905.220	10.94
LWR10517	4729.239	8.67	LWR15826	5452.553	7.55	LWP31038	9908.159	10.63
LWR10795	4762.162	8.81	LWR16023	5483.308	6.93	LWP31078	9912.134	10.38
LWR10854	4770.166	6.88	LWR16049	5486.227	7.75	LWP31093	9916.022	10.69
LWR10928	4778.162	8.00	LWR16120	5496.172	7.78	LWP31139	9920.166	8.35
LWR11603	4870.114	7.98	LWP09929	6809.583	7.83	LWP31161	9924.096	9.20
LWR11643	4878.035	9.32	LWP15073	7579.762	9.13	LWP31179	9928.164	8.22
LWR11762	4890.068	8.90	LWP15074	7579.795		LWP31206	9932.061	7.54
LWR11803	4896.049	7.97	LWP18561	8114.983	6.26	LWP31240	9936.058	9.42
LWR12906	5059.299	8.41	LWP30640	9845.381	9.93			
LWR12907	5059.328	8.06	LWP30691	9851.198	8.42			

**Note.** <sup>a</sup> *IUE* long wavelength primary/redundant camera, high dispersion, large aperture.

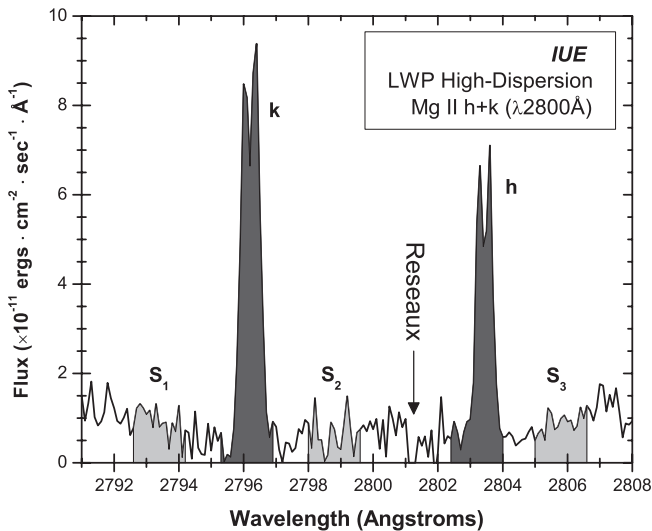


**Figure 10.** “Swatch” method similar to that used for the C IV analysis (see Figure 9) was implemented to determine emission flux strengths for the Mg II *h+k* (2803+2796 Å; 8,000–12,000 K; chromosphere) emission features. As described more thoroughly in the text, we have defined an Mg II Index by dividing the combined integrated fluxes found in the *h* and *k* emission line cores by a weighted average summation of integrated continuum values (swatches).

out that the maximum intrinsic S/N per pixel is  $\sim 12:1$ . Due to the manner by which adjacent pixels were grouped in low-resolution mode, Massa & Fitzpatrick (2000) demonstrate that an S/N  $\lesssim 30:1$  is ideally possible per spectral element. They also point to substantial systematic effects that remain in the *IUE* New Spectroscopic Image Processing System (NEWSIPS) data (used in this study), producing spectra that are only internally consistent to 10%–15%, at best. Unfortunately, the majority of these remaining systematics are time dependent. The flux sensitivity of the LWR camera, the worst case example, is shown to diminish by about 10% over its  $\sim 5$  years of service. Short-term temporal systematics also remain in the data, and can contribute to a “noise-like” uncertainty exceeding 10%.

In an attempt to assess the overall quality of the *IUE* data presented here, as it was reduced using the techniques outlined above, we selected several UV flux standard stars that were used as calibration standards for *HST* (see Bohlin et al. 1990). We measured all available spectra for the two stars that were the closest spectral type matches to  $\alpha$  Cen B, HD 186427 (G5 V) and HD 27836 (G1 V), along with the cool subgiant HD 2151 (G1 IV). We also subjected our reduction routines to sample spectra of the two *IUE* “prime standard” stars, HD 50753 (B3 IV) and HD 93521 (O9 V). With regards especially to the latter prime standard stars, these spectra were obtained uniformly throughout the life of the satellite, and therefore address the extent of the potentially remaining long- and short-term systematics in the NEWSIPS data, along with the internal consistencies (noisiness) within the individual *IUE* LWP/R and SWP spectra.

From this analysis we find that the internal consistency of the *IUE* NEWSIPS data, convolved with our method of data reduction, results in an uncertainty of better than about 20% for our integrated C IV line emission measures, and  $\lesssim 10\%$  for the individual Mg II *h+k* emission Index values. In addition, there were no discernable trends in the reduced spectra that were common to all of the measured standard stars that could have given rise to potential “false-positive” cycle determinations within the  $\alpha$  Cen B data set.

### 5.1. Long-term Magnetic Activity Cycle, Revisited

The long-lived (1978–1995) *IUE* satellite provides an opportunity to study  $\alpha$  Cen B’s magnetic activity over a relatively long period in the years preceding the current magnetic quiescence, as defined by the X-ray and FUV data described above (Sections 3 and 4). The results of the Lomb–Scargle periodogram analysis, with the complete C IV ( $\lambda 1550$  Å) and Mg II *h+k* ( $\sim \lambda 2800$  Å) data sets along with the entire X-ray luminosity measures, are shown in Figure 11. If we require an FDR of better than 20%, the intersection of the three FDR functions results in an expected long-term activity cycle between 7.96 and 9.22 years.

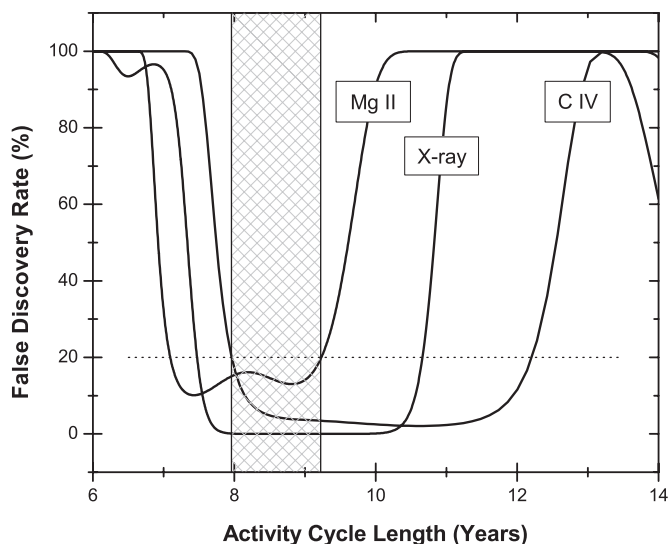


**Figure 11.** Long-term activity cycle false discovery rates (FDR) for all of the available *IUE* C IV emission and Mg II Index (1978–1995) data, along with the X-ray (*ROSAT*, *Chandra*, *XMM*) luminosity observations. Due to the temporally spasmodic nature of the acquired  $\alpha$  Cen B observations, narrow confinement of the overall activity cycle is not strictly possible, but considering the intersection of all FDR results together point to a possible range of about 7.96–9.22 years, with a better than 20% FDR.

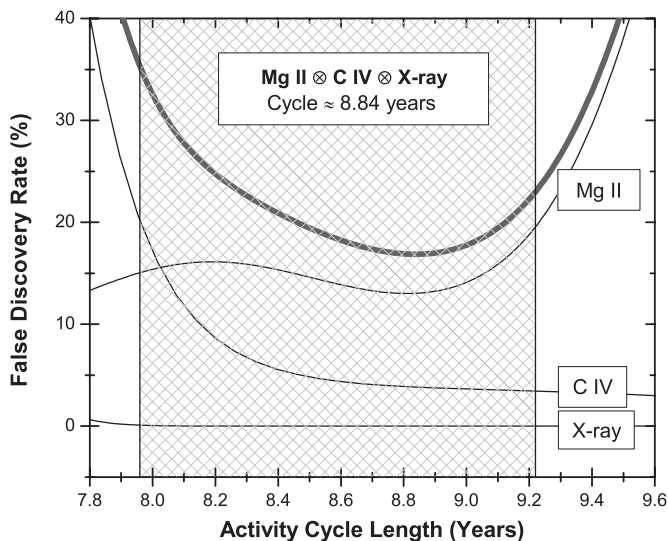


**Figure 12.** Convolution of the C IV emission, Mg II Index, and X-ray luminosity FDR functions result in a best determination of  $\sim 8.84$  yr (3230 days) for the long-term magnetic activity cycle for  $\alpha$  Cen B.

In their analysis of the Mg II data, Buccino & Mauas (2008) determine a long-term activity cycle of 8.38 yr (3061 days). Their procedure involved transforming the mean continuum flux near the Mg II  $h+k$  emission lines to the corresponding Mount Wilson Ca II HK  $\langle S \rangle$  index, which was then combined with optically determined values.

In this study, the convolution of all FDR distributions (see Figure 12) results in an “ultimate” best determination of  $P_{\text{cycle}} \approx 8.84$  years (3230 days) for the long-term activity cycle for  $\alpha$  Cen B. It should be noted, though, that strict comparison of the FDR functions for the individual X-ray and *IUE* data sets can be somewhat challenging. Though the *IUE* data is quantifiably noisier (producing less favorable FDRs), it encompasses multiple complete cycles (producing a much better constrained cycle duration).

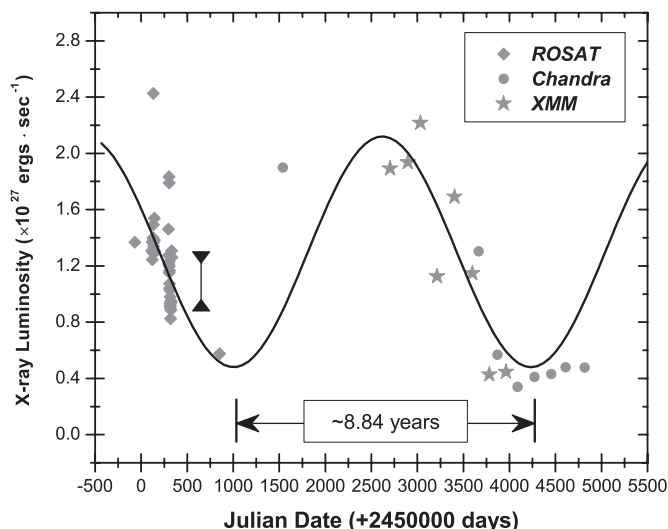


**Figure 13.** Displayed above are all available X-ray luminosity observations (1995–2008; gray symbols), converted into the common [0.2–2.0 keV] energy passband (see Ayres 2009). Uncertainties ( $\Delta L_X$ ) are typically of order  $\lesssim 4\%$  for the individual measures. Also shown is the appropriately modulated and phased light curve, as determined utilizing an iterative grid search method, incorporating the long-term magnetic activity cycle of  $\sim 8.84$  years as ascertained from all X-ray measures along with the *IUE* C IV emission and Mg II Index data. The vertical range bar near the *ROSAT* observations at  $\sim$ JD2450315 demonstrates the extent of the effects of rotational modulation of X-ray luminosity due to the presence of magnetically active regions or plages. Clearly, overall coronal X-ray luminosity is more affected by long-term magnetic activity changes than by the rotational modulation effects of discretely distributed active regions.

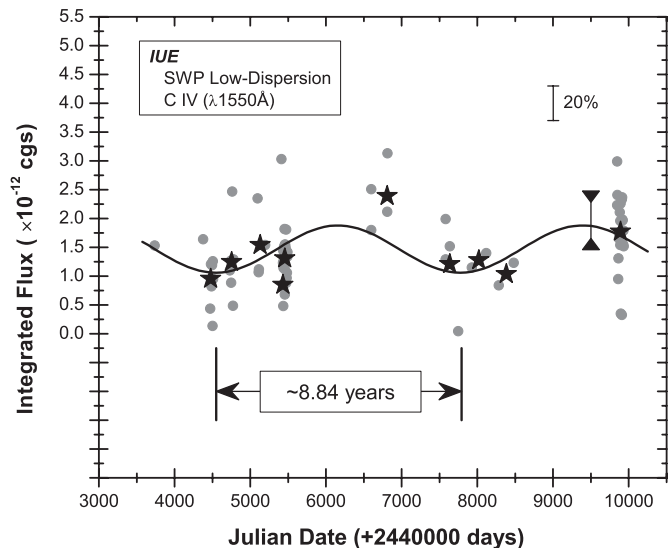


**Figure 14.** Data presented above include all available *IUE* C IV emission values (1978–1995; gray dots). The star symbols represent the  $\sim$ yearly averages. The long-term magnetic activity cycle (properly modulated and phased) of  $\sim 8.84$  years is evident and is determined with better than 15% FDR. Note that this cycle meshes precisely with the more contemporary X-ray observations (see Figure 13). A 20% uncertainty bar, our estimate of the internal consistency of the SWP C IV flux levels, is shown in the upper right corner. The vertical range bar near the observations at  $\sim$ JD2449900 demonstrates the extent of rotational modulation on the TR produced C IV emission levels.

An iterative grid search routine was employed to determine the appropriate light modulation amplitude and cycle phase for each of these data sets (X-ray, C IV, Mg II). Figure 13 shows the complete X-ray luminosity data set with the best-fitting, 8.84 year period, light curve. In Figure 14, the C IV data set is shown with the appropriately modulated and phased light

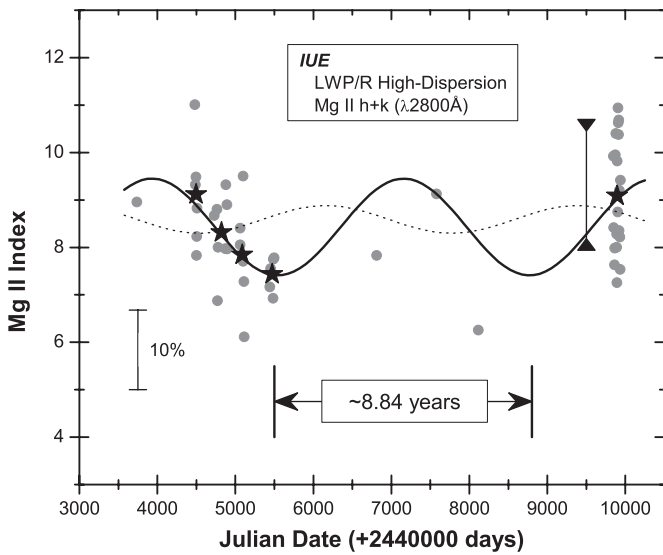


**Figure 15.** Data presented above include all available *IUE* Mg II  $h+k$  emission Index values (1978–1995; gray dots). The star symbols represent the  $\sim$ yearly averages. Though there is a lack of data in the important middle region of the above light curve, a long-term magnetic activity cycle of  $\sim$ 8.84 years would seem possible (solid line). A 10% uncertainty bar, our estimate of the internal consistency of the LWP/R Mg II emission Index values, is shown in the lower left corner. The vertical range bar near the observations at  $\sim$ JD2449900 demonstrates the extent of rotational modulation on the chromospherically produced Mg II  $h+k$  emission levels. Unlike the X-ray and C IV observations presented above (Figures 13 and 14), the effects of rotational modulation clearly dominate the overall emission level. Unfortunately, cycle phasing is significantly different to that of the X-ray and C IV observations (dashed line). It is unclear whether this measured activity cycle length is physical, but is unexpectedly not synchronized with activity levels in the hotter TR and corona, or if the randomly sampled rotational effects led to a serendipitous, albeit potentially spurious, determination.

curve overplotted. With regard to cycle phasing, no special consideration was necessary to mesh the X-ray and *IUE* C IV data correctly. As seen, the earlier C IV activity cycling phases directly into the more contemporary X-ray observations.

It must also be noted that contained within these long-term light curves are the rotational modulation effects of stellar active regions. As determined below (Section 5.2), the ratio of the long-term magnetic activity cycle amplitude to the rotational modulation amplitude ( $A_{\text{magnetic}}/A_{\text{rotation}}$ ) is about 3.9, 0.80, and  $\sim$ 0.5 for the X-ray, C IV, and Mg II observations, respectively. This implies that the X-ray data will be much more sensitive to the long-term magnetic activity changes than the rotational effects of active regions. Conversely, the Mg II Index appears to be the superior choice for more precisely determining  $\alpha$  Cen B's rotation period, yielding the highest determinacy.

The long-term chromospheric Mg II Index data set is shown in Figure 15. Though there is a paucity of data in the important middle regions of the timeline, the periodic cycling of  $\sim$ 8.84 years (via Lomb–Scargle analysis;  $\text{FDR} < 20\%$ ) would seem possible. Peculiarly, the computed best-fitting cycle phasing is significantly different to that of coronal X-ray and TR C IV observations ( $\Delta\phi/2\pi \approx 0.31$ , corresponding to a cycle phase lag of  $\sim$ 1000 days). An attempt was made to “split the difference” between the cycle phasing of the Mg II and that of both the C IV and X-ray data sets using the method of minimum phase dispersion, but this only resulted in a compromise that visually appeared inadequate for all three data sets.

It is possible that since the measured amplitude attributable to rotationally modulated Mg II  $h+k$  emission is significantly larger

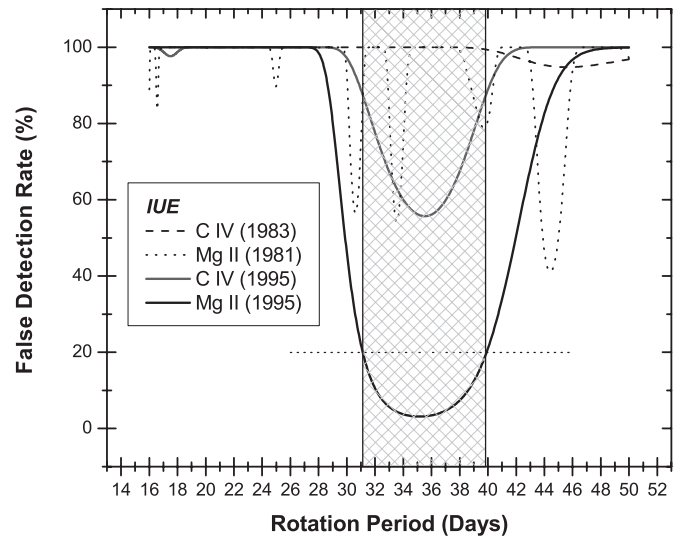


**Figure 16.** Plotted above is the false discovery rate (FDR) as a function of short-term light modulation period due to the presence of magnetically active regions. All potentially viable sections of *IUE* data are displayed. Only the Mg II Index data obtained in 1995 result in a rotation period of high confidence ( $P_{\text{rot}} \approx 35.1$  days;  $\text{FDR} \approx 5\%$ ), but as seen above, this solution is strongly corroborated by the 1995 C IV FDR result. Unfortunately, the other two epochs (1983 C IV; 1981 Mg II) were insufficiently sampled in phase space to obtain any additional useful rotation modulation information.

than the variability due to overall long-term chromospheric activity changes, that the effects of rotation modulation, combined with the insufficiently sampled data is overwhelming the effects attributable to long-term activity, resulting in a serendipitously measured  $\sim$ 8.8 year period. Alternatively, it is possible that this measured activity cycle length is indeed real and physical, but is simply not synchronized with activity levels in the hotter TR (C IV) and corona (X-ray). Considering the Sun's behavior in which the magnetic activity indicators are well-correlated (see, for example, Lean 1997; Judge et al. 2003), this latter scenario for  $\alpha$  Cen B must be considered unlikely.

### 5.2. Rotation Period, Revisited

The last *IUE* campaign in 1995 provides us with appropriate data sets to search for  $\alpha$  Cen B's rotation period, with sufficient observations of both Mg II  $h+k$  (20) and C IV (21) over the proper time frame ( $\sim$ 90 days). These observations were carried out by two of us (E.F.G. and L.E.D.) as part of an *IUE* GO program. Additionally, we explored potentially viable sections in 1981 (Mg II) and 1983 (C IV).

These *IUE* data sets were analyzed using the same Lomb–Scargle method described above. In Figure 16, the FDR functions for both spectral features observed during the 1995 campaign, along with the two other epochs that might have contained, a priori, marginally sufficient data, are displayed. As is apparent, the 1995 Mg II  $h+k$  Index data indicate a  $P_{\text{rotation}} = 35.1$  day rotation period for  $\alpha$  Cen B with a high level of confidence ( $\approx 3\%$  FDR). Due to the relatively broad nature of the FDR function, periods between about 31.1 and 39.9 days are plausible at the better than 20% FDR level. Though there is a higher degree of scatter (noise) within the data, the results of the analysis of the 1995 C IV flux variations substantively corroborate this 35.1 day rotation period, but with an expectedly higher predicted FDR. Figures 17 and 18 display the 1995 Mg II  $h+k$  Index and C IV emission flux data, respectively, overplotted with

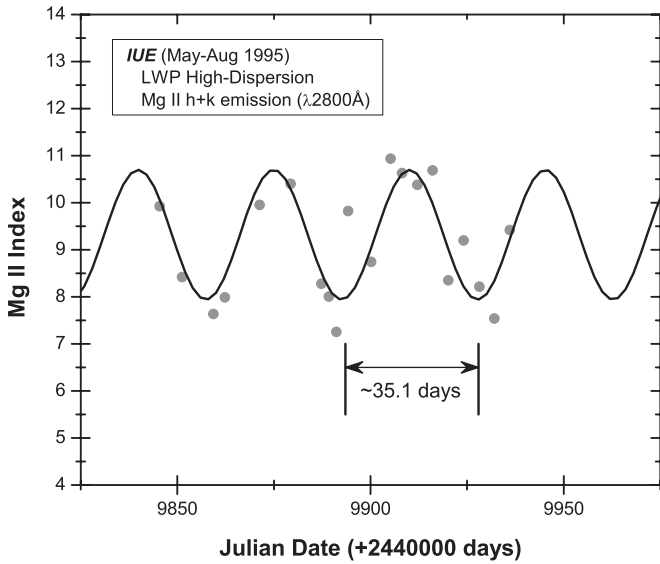


**Figure 17.** 1995 *IUE* Mg II Index values (gray dots) shown above are overplotted with the appropriately modulated and phased light curve, as determined utilizing an iterative grid search method and incorporating the  $\sim 35.1$  day rotation period ascertained from the above (see Figure 16) Lomb–Scargle analysis.

the appropriately modulated and phased light curve. Unfortunately, the 1981 and 1983 data sets were simply not adequately sampled, temporally, to derive any exacting rotation modulation information.

Previous spectroscopic determinations of the rotation rate of  $\alpha$  Cen B have been carried out by Jay et al. (1997;  $P_{\text{rotation}} = 36.9$  days), and Buccino & Mauas (2008; 35.1 days). These two previous studies wholly utilize the 1995 *IUE* data set(s), but employ different data reduction techniques than this study. Both (thankfully) arrive at essentially the same result as presented here. With regard to the possibility of spot (active region) creation/migration/destruction that may have occurred simultaneous to the observations, and/or the effects of differential rotation, the small differences between these rotation period values and that of the X-ray result above (Section 3.2; 37.8 days) must be considered negligible. Without prejudice to author or technique, the average rotation period of  $\alpha$  Cen B would therefore be  $P_{\text{rotation}} = 36.23 \pm 1.35$  days.

As insightfully pointed out by the anonymous referee: Saar & Osten (1997) infer a rotation period of 42 days for  $\alpha$  Cen B using an empirical relationship between the ratio of the chromospheric emission of the Mt. Wilson Ca II HK line cores to total bolometric emission,  $R'_{\text{HK}}$ , and the Rossby number,  $R_0$ , which is itself related to the rotation period of the star (see Noyes et al. 1984). The difference ( $\sim 14\%$ ) in the rotation period determined in this study and the estimate of Saar & Osten (1997) is likely in part due to intrinsic scatter in  $R'_{\text{HK}}$  at a given  $R_0$  (due to rotational modulation, activity cycles), plus problems in calibration of the  $R'_{\text{HK}} - R_0$  relationship, especially at low activity levels (Wright 2004; Pace & Pasquini 2004; Saffe et al. 2005; Saar 2006). In particular, clear trends with metallicity are not included in the standard (Noyes et al. 1984) calibration (Wright 2004; Saar 2006).  $\alpha$  Cen B is rather metal rich, which pushes the inferred minimum  $R'_{\text{HK}}$  (and likely the whole calibration) to overly low values (Saar 2006). With  $R'_{\text{HK}}$  too low (due to uncalibrated high metals), the  $P_{\text{rotation}}$  derived from  $R'_{\text{HK}}$  would be too large, as seen.

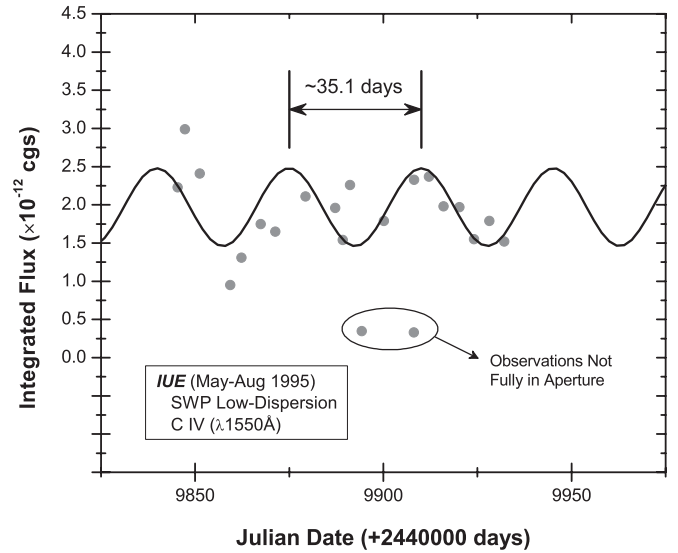


**Figure 18.** As seen above, the determined  $\sim 35.1$  day rotation rate (properly modulated and phased) appears appropriate for the 1995 *IUE* C IV emission data (gray dots). Unfortunately, due to the clearly higher degree of noise within these observations, high confidence is not, per se, possible.

## 6. STATISTICAL TREATMENT OF PERIOD FDRS

To further address the robustness of the analytically derived Lomb–Scargle FDRs presented throughout this paper, Monte Carlo random permutation simulations (see Dwass 1957) were carried out. Random permutation tests are restricted to cases where changing the temporal order of the data destroys the measured effect. In our case, power is the test statistic, since it is power that leads directly to the FDR value.

The technique involves randomly rearranging the data points, leaving the time spacing the same, rerunning the periodogram, and keeping track of the number of instances that the resultant power is greater than the original value. There are too many possible orderings to allow complete enumeration with the number of data points used in our respective period determinations, but fortunately, as pointed out by Dwass (1957), the Monte Carlo simulations are asymptotically equivalent to the full permutation test, provided the number of iterations is sufficiently large.

For our tests, the number of iterations was always  $N = 100,000$ . In all cases the resultant power frequency distributions were well represented with Gamma probability distributions that could be characterized by the standard shape ( $k$ ) and scale ( $\theta$ ) parameters, with a small offset (shift) along the power axis ( $X_0$ ). For these Gamma probability distribution, the mean power is then given by  $k \times \theta + X_0$ . The statistical  $p$ -value represents the fractional number of permutations that resulted in a greater power, and correspondingly better FDR. Therefore,

$$p\text{-value} = 1 - \text{cdf},$$

where cdf is the cumulative distribution function appropriate to the resultant Gamma probability distribution, evaluated at the desired power (minus  $X_0$ ). Shown in Figure 19 is the power frequency distribution for the 1995 *IUE* C IV data set (used for the determination of  $\alpha$  Cen B's rotation rate), which incidentally has the highest (aka poorest) FDR reported in this study. As seen, the Monte Carlo random permutation test results in a “true” statistical FDR of  $\sim 53\%$ , compared to the  $\sim 61\%$  reported by Lomb–Scargle.

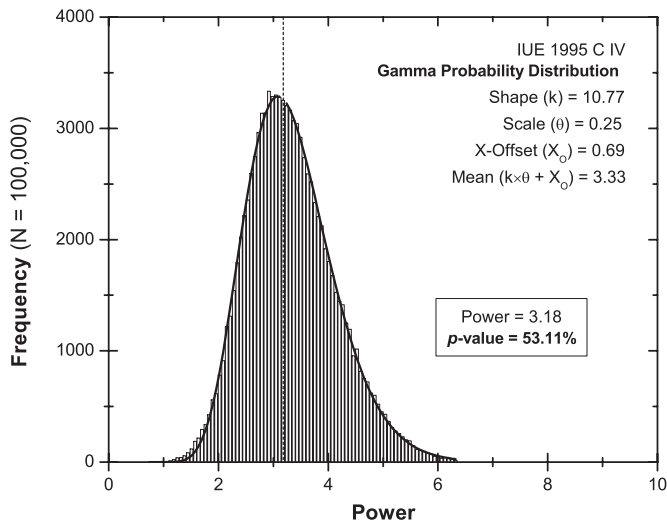


**Figure 19.** Results of the Monte Carlo permutation test for the 1995 *IUE* C IV data set. The number of iterations was 100,000, and the resultant power frequency is well represented with a Gamma probability distribution characterized by the standard shape ( $k$ ) and scale ( $\theta$ ) parameters, along with a small offset (shift) along the power axis ( $X_0$ ). For this type of distribution, the mean power is then given by  $k \times \theta + X_0$ . The statistical  $p$ -value represents the fractional number of permutations that result in a greater power, and in this case,  $p$ -value =  $1 - \text{cdf}$ , where  $\text{cdf}$  is the cumulative distribution function of the resultant Gamma probability distribution, evaluated at the desired power (minus  $X_0$ ). For this data set, the Lomb–Scargle period analysis results in a rotation rate of 35.1 days with a power of 3.18 and an analytically derived FDR of 60.5%. The Monte Carlo permutation analysis shown above implies that the Lomb–Scargle FDR is comparable, but overestimates the statistically derived false detection rate ( $p$ -value  $\approx$  53.11%).

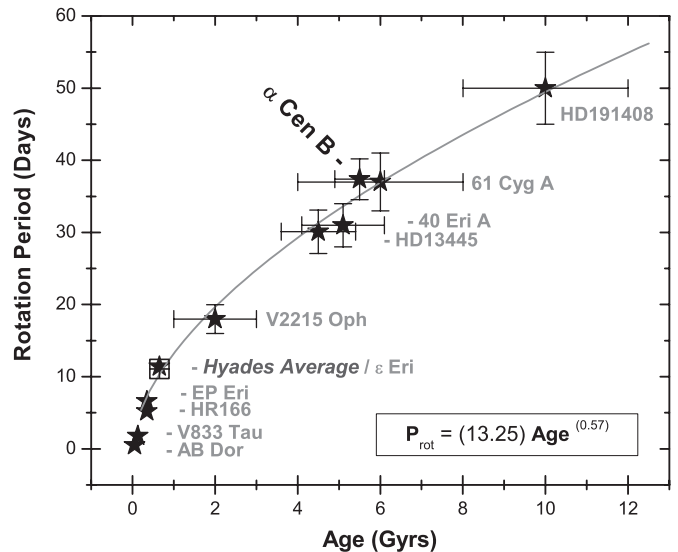


**Figure 20.** Shown above is a plot of rotation period vs. age for a sample of our program dK stars. The box symbol represents the weighted average rotation rate value for nine Hyades K0–K5 V stars (Radick et al. 1987). Most of all stars displayed above have well-determined ages and independently measured rotation periods (see Table 1). The line represents the best-fitting power-law relation to these data and its functional dependence is given in the figure. Note that the rotation period result ( $P_{\text{rot}} = 36.23 \pm 1.35$  days) presented in this study for  $\alpha$  Cen B agrees well with expectations for a typical 5.6 Gyr K1 V star.

**Table 9**

Statistical Treatment of False Detection Rates

Data Set	Period <sup>a</sup>	Lomb–Scargle		Monte Carlo Permutation Test				
		Power <sup>b</sup>	FDR <sup>c</sup>	$k$ (shape)	$\theta$ (scale)	$X_0$	Mean <sup>d</sup>	$p$ -value <sup>e</sup>
Long-term magnetic activity cycle								
X-ray	3230	16.90	$\approx 0$	5.96	0.53	0.28	3.44	$\approx 0$
C IV	3230	7.75	3.8	5.17	0.62	0.46	3.69	1.14
Mg II	3230	5.96	13.0	4.89	0.63	0.14	3.24	4.44
Rotation modulation								
X-ray	37.8	10.11	0.1	5.88	0.40	1.21	3.59	$\approx 0$
C IV	35.1	3.18	60.5	10.77	0.25	0.69	3.33	53.11
Mg II	35.1	6.28	4.9	6.16	0.38	1.15	3.47	0.85

**Notes.**

- <sup>a</sup> Reported period value in days.
- <sup>b</sup> Measured Lomb–Scargle power of the reported period value.
- <sup>c</sup> Analytically derived false detection rate determined by the Lomb–Scargle analysis.
- <sup>d</sup> For the resultant Gamma probability distributions, the mean power =  $k \times \theta + X_0$ .
- <sup>e</sup> Fractional number of permutations that result in a higher measured power. In this case,  $p$ -value =  $1 - \text{cdf}$ , where  $\text{cdf}$  is the cumulative distribution function of the resultant Gamma probability distribution, evaluated at the measured power, offset by  $-X_0$ .

The results of all of the Monte Carlo simulations are shown in Table 9 along with the respective Lomb–Scargle FDR values. Note that the analytically determined values given by the Lomb–Scargle method appear to be comparable to the values given by the Monte Carlo simulations, but consistently overestimate the statistical FDRs.

**7. CONCLUSIONS**

Independent analyses on the essentially complete sets of X-ray and FUV observations, along with the extensive *IUE* UV/NUV data sets, have yielded determinations of the long-term magnetic activity cycle length ( $P_{\text{cycle}} = 8.84 \pm 0.4$  yr) and the rotation period ( $P_{\text{rotation}} = 36.2 \pm 1.4$  days) of the nearby K dwarf,  $\alpha$  Cen B. Figure 20 places  $\alpha$  Cen B in context with the other stars in our dK star program (see also Table 1). We note that the rotation period result determined within this study agrees well with expectations for a typical 5.6 Gyr K1 V star.

Since our *FUSE* Cycles 7 and 8 observations occurred after the failure of two reaction wheels in 2001 December, there were some additional “difficulties” for *FUSE* pointing and acquisition. Fortunately (all credit is due to the heroic efforts of the *FUSE* team—battling roll angles, drift, and jitter), the individual spectra of  $\alpha$  Cen A and B were ultimately secured. B-G Andersson was also of great individual help in the preparation, acquisition, and analysis stages. We also thank Tom Woods (*LASP*, UC Boulder) for his assistance and expertise with the extraction and interpretation of the *Solar EUV Experiment* data used herein. In addition, we gratefully acknowledge comments and observations made by the anonymous referee and support by NASA Grants NNX06AC45G, NNX08AG95G, and the Villanova University Research for Undergraduates Award Program.

**REFERENCES**

Acton, L. W. 1996, in ASP Conf. Ser. 109, Cool Stars, Stellar Systems and the Sun, ed. R. Pallavicini & A. K. Dupree (San Francisco, CA: ASP), 45  
 Anosova, J., Orlov, V. V., & Pavlova, N. A. 1994, *A&A*, 292, 115  
 Ayres, T. R. 1993, *PASP*, 105, 538  
 Ayres, T. R. 1997, *J. Geophys. Res.*, 102, 1641  
 Ayres, T. R. 2009, *ApJ*, 696, 1931  
 Baliunas, S. L., et al. 1995, *ApJ*, 438, 269

- Bean, J., McArthur, B. E., & Benedict, G. F. 2006, *BAAS*, **38**, 932
- Benedict, G. F. 2008, *BAAS*, **40**, 263
- Benedict, G. F., McArthur, B. E., & Bean, J. L. 2008, in *IAU Symp. 248, A Giant Step: from Milli- to Micro-arcsecond Astrometry*, ed. W. J. Jin, I. Platais, & M. A. C. Perryman (Cambridge: Cambridge Univ. Press), 23
- Benedict, G. F., et al. 1999, *AJ*, **118**, 1086
- Benest, D. 1988, *A&A*, **206**, 143
- Bohlin, R. C., Harris, A. W., Holm, A. V., & Gry, C. 1990, *ApJS*, **73**, 413
- Bonavita, M., & Desidera, S. 2007, *A&A*, **468**, 721
- Buccino, A. P., & Mauas, P. J. D. 2008, *A&A*, **483**, 903
- Chmielewski, Y., Friel, E., Cayrel de Strobel, G., & Bentolila, C. 1992, *A&A*, **263**, 219
- Coughlin, J., Guinan, E. F., Engle, S. G., DeWarf, L., Hall, J. C., DePasquale, J., & Thompson, R. R. 2010, *BAAS*, **42**, 333
- Crawford, D. L., Barnes, J. V., & Golson, J. C. 1970, *AJ*, **75**, 624
- Demarque, P., Guenther, D. B., & van Altena, W. F. 1986, *ApJ*, **300**, 773
- Dorren, J. D., & Guinan, E. F. 1994a, in *IAU Coll. 143, The Sun as a Variable Star: Solar and Stellar Irradiance Variations*, ed. J. M. Pap et al. (Cambridge: Cambridge Univ. Press), 206
- Dorren, J. D., & Guinan, E. F. 1994b, *ApJ*, **428**, 805
- Dorren, J. D., Guinan, E. F., & DeWarf, L. E. 1994, in *Proc. Eighth Cambridge Workshop, Vol. 64, Cool Stars, Stellar Systems, and the Sun*, ed. J.-P. Caillault (Dordrecht: Kluwer), 399
- Doyle, J. G., Raymond, J. C., Noyes, R. W., & Kingston, A. E. 1985, *ApJ*, **297**, 816
- Doyle, M. T., O'Mara, B. J., Ross, J. E., & Bessell, M. S. 2005, *PASA*, **22**, 6
- Dupree, A. K., Foukal, P. V., & Jordan, C. 1976, *ApJ*, **209**, 621
- Dwass, M. 1957, *Ann. Math. Stat.*, **28**, 181
- Eggen, O. J. 1978a, *ApJ*, **226**, 405
- Eggen, O. J. 1978b, *ApJS*, **37**, 251
- Eggen, O. J. 1996, *AJ*, **111**, 466
- Eggenberger, P., Charbonnel, C., Talon, S., Meynet, G., Maeder, A., Carrier, F., & Bourban, G. 2004, *A&A*, **417**, 235
- Endl, M., & Kürster, M. 2008, *A&A*, **488**, 1149
- Endl, M., Kürster, M., Els, S., Hatzes, A. P., & Cochran, W. D. 2001, *A&A*, **374**, 675
- Engle, S. G., Guinan, E. F., & Mizusawa, T. 2009, in *AIP Conf. Proc. 1135, Future Directions in Ultraviolet Spectroscopy*, ed. M. E. Van Steenberg et al. (Melville, NY: AIP), 221
- Favata, F., Micela, G., Orlando, S., Schmitt, J. H. M. M., Sciortino, S., & Hall, J. 2008, *A&A*, **490**, 1121
- Flannery, B. P., & Ayres, T. R. 1978, *ApJ*, **221**, 175
- Furenlid, I., & Meylan, T. 1990, *ApJ*, **350**, 827
- Giménez, A. 2000, *A&A*, **356**, 213
- Golub, L., Harnden, F. R., Jr., Pallavicini, R., Rosner, R., & Vaiana, G. S. 1982, *ApJ*, **253**, 242
- Grißmeier, J.-M., et al. 2004, *A&A*, **425**, 753
- Güdel, M., Guinan, E. F., & Skinner, S. L. 1997, *ApJ*, **483**, 947
- Güdel, M., Guinan, E. F., & Skinner, S. L. 1998, in *ASP Conf. Ser. 154, Cool Stars, Stellar Systems and the Sun*, ed. R. A. Donahue & J. A. Bookbinder (San Francisco, CA: ASP), 1041
- Guedes, J. M., Rivera, E. J., Davis, E., Laughlin, G., Quintana, E. V., & Fischer, D. A. 2008, *ApJ*, **679**, 1582
- Guenther, D. B., & Demarque, P. 2000, *ApJ*, **531**, 503
- Guinan, E. F., Engle, S. G., & DeWarf, L. E. 2009, in *AIP Conf. Proc. 1135, Future Directions in Ultraviolet Spectroscopy*, ed. M. E. Van Steenberg et al. (Melville, NY: AIP), 244
- Guinan, E. F., Ribas, I., & Harper, G. M. 2003, *ApJ*, **594**, 561
- Haisch, B., & Schmitt, J. H. M. M. 1996, *PASP*, **108**, 113
- Halliwell, M. 1981, *ApJS*, **47**, 243
- Hatzes, A. P., Kürster, M., Cochran, W. D., Dennerl, K., & Döbereiner, S. 1996, *J. Geophys. Res.*, **101**, 9285
- Hoffleit, D., & Jaschek, C. 1982, *The Bright Star Catalogue* (4th ed.; New Haven, CT: Yale Univ. Observatory)
- Horne, J. H., & Baliunas, S. L. 1986, *ApJ*, **302**, 757
- Jay, J. E., Guinan, E. F., Morgan, N. D., Messina, S., & Jassour, D. 1997, *BAAS*, **29**, 730
- Judge, P. G., Solomon, S. C., & Ayres, T. R. 2003, *ApJ*, **593**, 534
- Kervella, P., Thévenin, F., Segransan, D., Berthomieu, G., Lopez, B., Morel, P., & Provost, J. 2003, *A&A*, **404**, 1087
- Komitov, B., Duchlev, P., Stoychev, K., Dechev, M., & Koleva, K. 2010, arXiv:1008.0375v1
- Kulikov, Y. N., et al. 2006, *Planet. Space Sci.*, **54**, 1425
- Kürster, M., Hatzes, A. P., Cochran, W. D., Döbereiner, S., Dennerl, K., & Endl, M. 1999, *A&A*, **344**, L5
- Lammer, H., Lichtenegger, H. I. M., Kolb, C., Ribas, I., Guinan, E. F., Abart, R., & Bauer, S. J. 2003a, *Icarus*, **165**, 9
- Lammer, H., Selsis, F., Ribas, I., Guinan, E. F., Bauer, S. J., & Weiss, W. W. 2003b, *ApJ*, **598**, 121
- Lean, J. 1991, *Rev. Geophys.*, **29**, 505
- Lean, J. 1997, *ARA&A*, **35**, 33
- Lomb, N. R. 1976, *Ap&SS*, **39**, 447
- Massa, D., & Fitzpatrick, E. L. 2000, *ApJS*, **126**, 517
- Micela, G., & Marino, A. 2003, *A&A*, **404**, 637
- Morel, P., Provost, J., Lebreton, Y., Thévenin, F., & Berthomieu, G. 2000, *A&A*, **363**, 675
- Murdoch, K. A., Hearnshaw, J. B., & Clark, M. 1993, *ApJ*, **413**, 349
- Neuforge-Verheecke, C., & Magain, P. 1997, *A&A*, **328**, 261
- Noyes, R. W., Hartmann, L. W., Baliunas, S. L., Duncan, D. K., & Vaughan, A. H. 1984, *ApJ*, **279**, 763
- Noyes, R. W., Raymond, J. C., Doyle, J. G., & Kingston, A. E. 1985, *ApJ*, **297**, 805
- Orlando, S., Peres, G., & Reale, F. 2001, *ApJ*, **560**, 499
- Pace, G., & Pasquini, L. 2004, *A&A*, **426**, 1021
- Pallavicini, R., Golub, L., Rosner, R., & Vaiana, G. 1981, in *Proc. Second Cambridge Workshop, Cool Stars, Stellar Systems, and the Sun*, Vol. 2, ed. G. M. Giampapa & L. Golub (Cambridge, MA: Smithsonian Astroph. Obs.), 77
- Perryman, M. A. C., et al. 1997, *A&A*, **323**, L49
- Pettersen, B. R. 1980, *A&A*, **82**, 53
- Porto de Mello, G. F., Lyra, W., & Keller, G. R. 2008, *A&A*, **488**, 653
- Pourbaix, D., Neuforge-Verheecke, C., & Noels, A. 1999, *A&A*, **344**, 172
- Pourbaix, D., et al. 2002, *A&A*, **386**, 280
- Press, W. H., & Rybicki, G. B. 1989, *ApJ*, **338**, 277
- Quintana, E. V., Adams, F. C., Lissauer, J. J., & Chambers, J. E. 2007, *ApJ*, **660**, 807
- Raassen, A. J. J., Ness, J.-U., Mewe, R., van der Meer, R. L. J., Burwitz, V., & Kaastra, J. S. 2003, *A&A*, **400**, 671
- Radick, R. R., Thompson, D. T., Lockwood, G. W., Duncan, D. K., & Baggett, W. E. 1987, *ApJ*, **321**, 459
- Ribas, I., Guinan, E. F., Güdel, M., & Audard, M. 2005, *ApJ*, **622**, 680
- Robrade, J., Schmitt, J. H. M. M., & Favata, F. 2005, *A&A*, **442**, 315
- Robrade, J., Schmitt, J. H. M. M., & Hempelmann, A. 2007, *Mem. Soc. Astron. Ital.*, **78**, 311
- Rutten, R. G. M., & Schrijver, C. J. 1987, *A&A*, **177**, 155
- Saar, S. H. 2006, *BAAS*, **38**, 240
- Saar, S. H., & Osten, R. A. 1997, *MNRAS*, **284**, 803
- Saffe, C., Gómez, M., & Chavero, C. 2005, *A&A*, **443**, 609
- Scargle, J. D. 1982, *ApJ*, **263**, 835
- Schmitt, J. H. M. M. 1997, *A&A*, **318**, 215
- Schrijver, C. J. 1983, *A&A*, **127**, 289
- Ségransan, D., Kervella, P., Forveille, T., & Queloz, D. 2003, *A&A*, **397**, L5
- Soederhjelm, S. 1999, *A&A*, **341**, 121
- Solanki, S. K., Usoskin, I. G., Kromer, B., Schüssler, M., & Beer, J. 2004, *Nature*, **431**, 1084
- Thebault, P., Marzari, F., & Scholl, H. 2009, *MNRAS*, **393**, 21
- Thévenin, F., Provost, J., Morel, P., Berthomieu, G., Bouchy, F., & Carrier, F. 2002, *A&A*, **392**, 9L
- Vaiana, G. S., & Rosner, R. 1978, *ARA&A*, **16**, 393
- van Leeuwen, F. 2007, *Hipparcos, the New Reduction of the Raw Data* (Astrophys. Space Sci. Lib. 350; Dordrecht: Springer)
- Wiegert, P. A., & Holman, M. J. 1997, *AJ*, **113**, 1445
- Woods, T. N., et al. 2005, *J. Geophys. Res.*, **110**, A01312
- Wright, J. T. 2004, *AJ*, **128**, 1273
- Wyatt, M. C., Clarke, C. J., & Greaves, J. S. 2007, *MNRAS*, **380**, 1737
- Yildiz, M. 2007, *MNRAS*, **374**, 1264
- Yildiz, M. 2008, *MNRAS*, **388**, 1143